Diazapyrenium-containing catenanes and rotaxanes‡

Peter R. Ashton,[a] Sue E. Boyd,[a] Alexander Brindle,[a] Steven J. Langford,[a] Stephan Menzer,[b] Lluisa Pérez-Garcia,[a] Jon A. Preece,[a] Françisco M. Raymo,†[a] Neil Spencer,[a] J. Fraser Stoddart,*†[a] Andrew J. P. White[b] and David J. Williams[b]

[a] *School of Chemistry, University of Birmingham, Edgbaston, Birmingham, UK B15 2TT. E-mail: stoddart@chem.ucla.edu*

[b] *Department of Chemistry, Imperial College, South Kensington, London, UK SW7 2AY*

Received (in Cambridge) 1st December 1998, Accepted 9th February 1999

Diazapyrenium units have been incorporated into the π-electron deficient components of four [2]pseudorotaxanes, four [2]catenanes, and two [2]rotaxanes, each having a dioxyarene-based macrocyclic polyether as the π-electron rich component. A dramatic increase in the association constants that characterize the formation of diazapyrenium-containing [2]pseudorotaxanes, relative to those of their bipyridinium-based analogs, was observed in solution studies. These results indicate that the intercomponent non-covalent bonding interactions are reinforced significantly when diazapyrenium, instead of bipyridinium, recognition sites are employed in the π-electron deficient components of this kind of [2]pseudorotaxane. Not surprisingly, therefore, in two asymmetric [2]catenanes which incorporate one diazapyrenium and one bipyridinium recognition site within their tetracationic cyclophane components, the diazapyrenium unit is located inside the cavity of the π-electron rich macrocyclic component as revealed in the solid state by X-ray crystallographic analyses and by ^{1}H NMR spectroscopic studies in solution. Variable temperature ^{1}H NMR spectroscopic studies showed that, in the [2]catenanes, the free energy barriers associated with the circumrotation of one macrocyclic component through the cavity of the other and *vice versa* increase when diazapyrenium, instead of bipyridinium, recognition sites are employed, reflecting the stronger intercomponent non-covalent bonding interactions involving the former.

Introduction

Mechanically interlocked[1] molecules and their supramolecular analogs can be constructed efficiently by relying upon non-covalent bonding interactions between appropriate recognition sites. To this end, a combination of [C–H···O] hydrogen bonds, [π···π] stacking, and [C–H···π] interactions has been exploited[2] in the syntheses of catenanes and rotaxanes incorporating bipyridinium-based components mechanically interlocked with dioxyarene-based polyether components. In these systems, the α-bipyridinium protons sustain [C–H···O] hydrogen bonds with the polyether oxygen atoms. In addition, the π-electron deficient bipyridinium recognition sites [π···π] stack with the π-electron rich dioxyarene units. Preliminary studies suggested[3] that these non-covalent bonding interactions can be reinforced by replacing the bipyridinium units with diazapyrenium recognition sites. Here, we report (*i*) the syntheses of a number of acyclic and cyclic diazapyrenium-containing compounds, (*ii*) their incorporation into four [2]pseudorotaxanes, four [2]catenanes, and two [2]rotaxanes, (*iii*) the X-ray crystallographic analyses of all four [2]pseudorotaxanes, and of two of the four [2]catenanes, as well as of the tetracationic cyclophane containing one bipyridinium and one diazapyrenium unit and of 2,7-dibenzyldiazapyrenium bis(hexafluorophosphate), and (*iv*) the variable temperature ^{1}H NMR spectroscopic investigations of all of the [2]catenanes and of both of the [2]rotaxanes.

Results and discussion

Synthesis

The conversion of **1** into **2** was achieved (Scheme 1) in three steps in an overall yield of 43% following a modified literature procedure.[4] Alkylation of **2** with MeI, $PhCH_2Br$, or **5**, followed by counterion exchange, gave the compounds **3**·2PF_6, **4**·2PF_6, **6**·2PF_6, and **7**·2PF_6 in good yields (59–95%). The diazapyrenium-containing compounds **3**·2PF_6 and **4**·2PF_6, as well as the bipyridinium-containing one **8**·2PF_6,[5,6] are bound (Scheme 2) by the macrocyclic polyether **9** or **10** with pseudorotaxane geometries in CD_3CN. The corresponding association constants (K_a) were determined by either ^{1}H NMR or absorption UV-VIS spectroscopy, using dilution or titration procedures,[7] respectively. Higher K_a values are observed (Table 1) when (*i*) 1,5-dioxynaphthalene instead of 1,4-dioxybenzene recognition sites are incorporated into the host, (*ii*) a diazapyrenium instead of a bipyridinium recognition site is present in the guest, and (*iii*) the guest carries benzyl instead of methyl substituents.

Macrocyclization of either **6**·2PF_6 and **11** or **2** and **12**·2PF_6 in the presence of the template **13** afforded (Scheme 3) the diazapyrenium-based cyclophane **14**·4PF_6 in yields of 30 or 59%, respectively. Similarly, macrocyclization of **6**·2PF_6 and **2** in the presence of the template **15** gave (Scheme 4) the diazapyrenium-based cyclophane **16**·4PF_6 in a yield of 51%. When a macrocyclic polyether template (either **9** or **10**) was employed (Schemes 5 and 6) under similar conditions, the

† *Present address*: Department of Chemistry and Biochemistry, University of California, Los Angeles, 405 Hilgard Avenue, Los Angeles, CA 90095-1569, USA.

‡ "Molecular Meccano", Part 50: for Part 49, see: M. Asakawa, P. R. Ashton, V. Balzani, S. E. Boyd, A. Credi, G. Mattersteig, S. Menzer, M. Montalti, F. M. Raymo, C. Ruffilli, J. F. Stoddart, M. Venturi and D. J. Williams, *Eur. J. Org. Chem.*, 1999, 985.

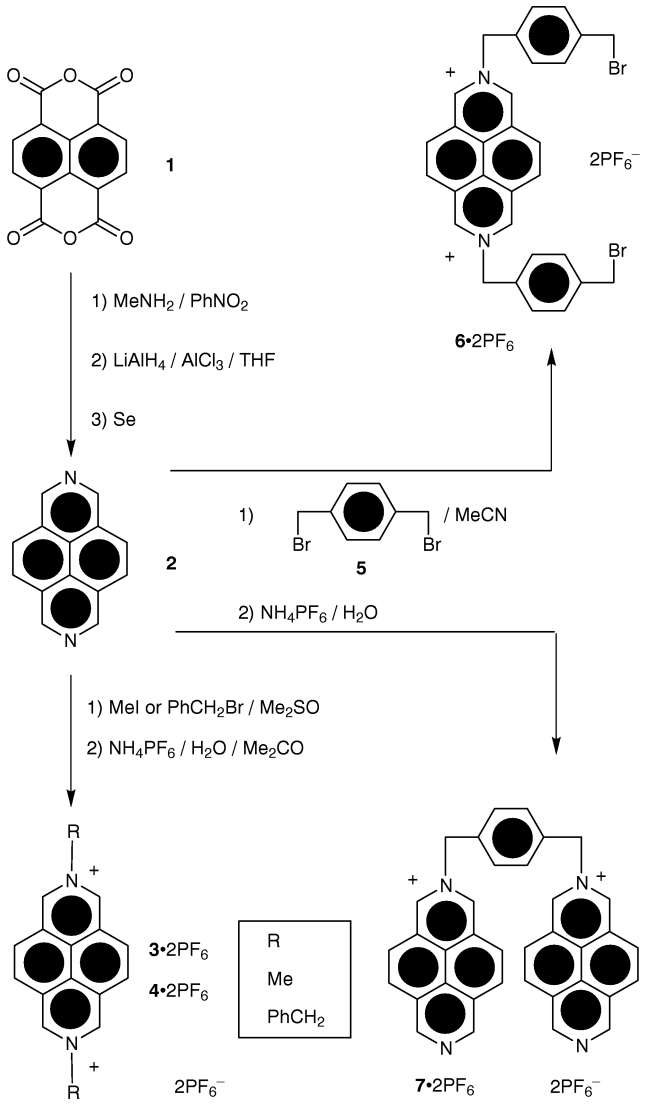

Scheme 1 Synthesis of the diazapyrenium-containing compounds $3 \cdot 2PF_6$, $4 \cdot 2PF_6$, $6 \cdot 2PF_6$, and $7 \cdot 2PF_6$.

[2]catenanes $17 \cdot 4PF_6$–$20 \cdot 4PF_6$ were isolated in good yields (37–73%) after counterion exchange. Reaction of **21** with 2-[2-(2-chloroethoxy)ethoxy]ethanol, followed by tosylation and alkylation, gave (Scheme 7) the dumbbell-shaped compound **25** in an overall yield of 25%. This compound was employed (Scheme 8) to template the macrocyclization of **5** and $7 \cdot 2PF_6$, as well as that of **5** and $26 \cdot 2PF_6$, which gave the corresponding [2]rotaxanes $27 \cdot 4PF_6$ and $28 \cdot 4PF_6$ in yields of 43 and 23%, respectively, after counterion exchange. The alkylation of **2** with **29** was carried out in the presence of **9** and under high pressure (12 kbar) conditions to afford (Scheme 9) the

Table 1 Association constants (K_a) and derived free energies of association ($-\Delta G°$) for the complexes $[3 \cdot 9] \cdot 2PF_6$, $[3 \cdot 10] \cdot 2PF_6$, $[4 \cdot 9] \cdot 2PF_6$, $[4 \cdot 10] \cdot 2PF_6$, $[8 \cdot 9] \cdot 2PF_6$ and $[8 \cdot 10] \cdot 2PF_6$ in CD_3CN at 25 °C

Complex	K_a/dm^3 mol^{-1}	$-\Delta G°$/kcal mol^{-1}
$[3 \cdot 9] \cdot 2PF_6$	5900 ± 400[a]	5.1 ± 0.2
$[3 \cdot 10] \cdot 2PF_6$	11000 ± 1000[a]	5.5 ± 0.1
$[4 \cdot 9] \cdot 2PF_6$	29000 ± 8000[b]	6.1 ± 0.2
$[4 \cdot 10] \cdot 2PF_6$	290000 ± 60000[b]	7.5 ± 0.2
$[8 \cdot 9] \cdot 2PF_6$	240 ± 40[a]	3.3 ± 0.1
$[8 \cdot 10] \cdot 2PF_6$	670 ± 30[b]	3.8 ± 0.1

[a] Determined by ^{1}H NMR spectroscopy using the dilution procedure. [b] Determined by absorption UV-VIS spectroscopy using the titration procedure.

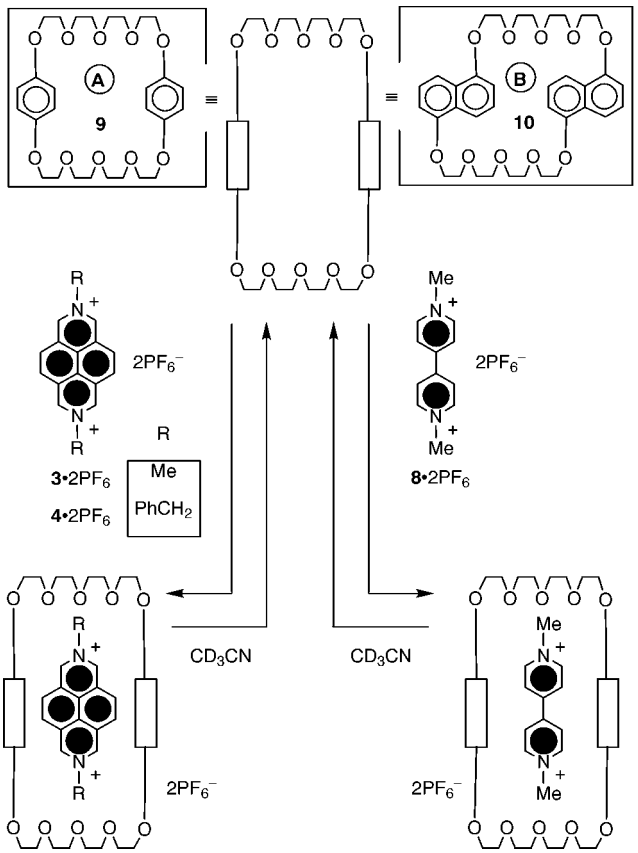

Scheme 2 Complexation of the dicationic compounds $3 \cdot 2PF_6$, $4 \cdot 2PF_6$, and $8 \cdot 2PF_6$ by the macrocyclic polyethers **9** and **10**.

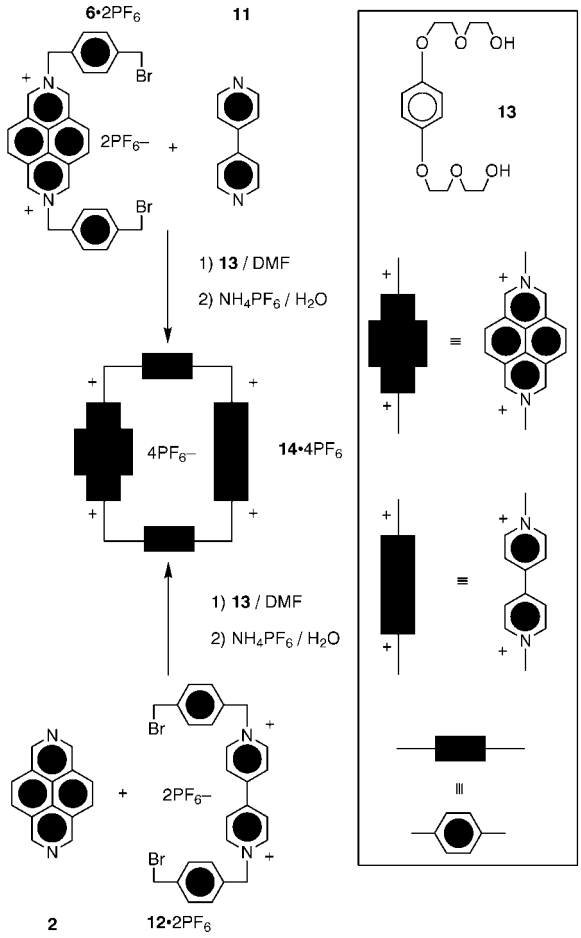

Scheme 3 Template-directed synthesis of the diazapyrenium-containing cyclophane $14 \cdot 4PF_6$.

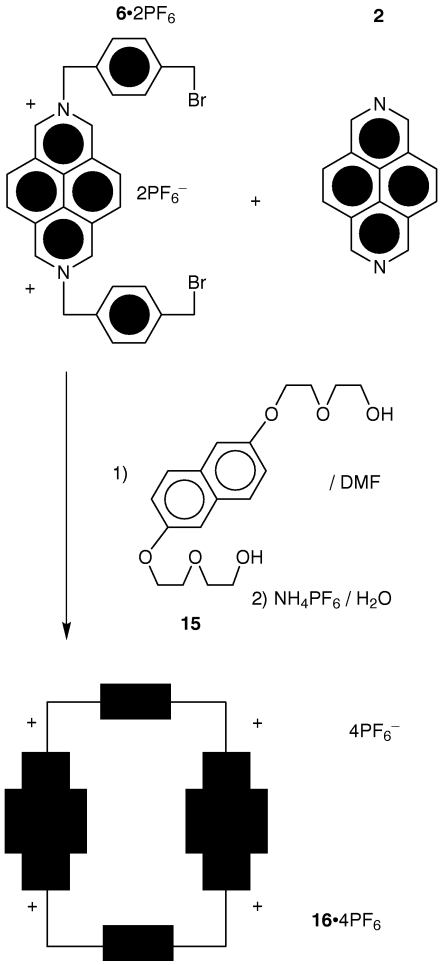

Scheme 4 Template-directed synthesis of the diazapyrenium-containing cyclophane $\mathbf{16} \cdot 4PF_6$.

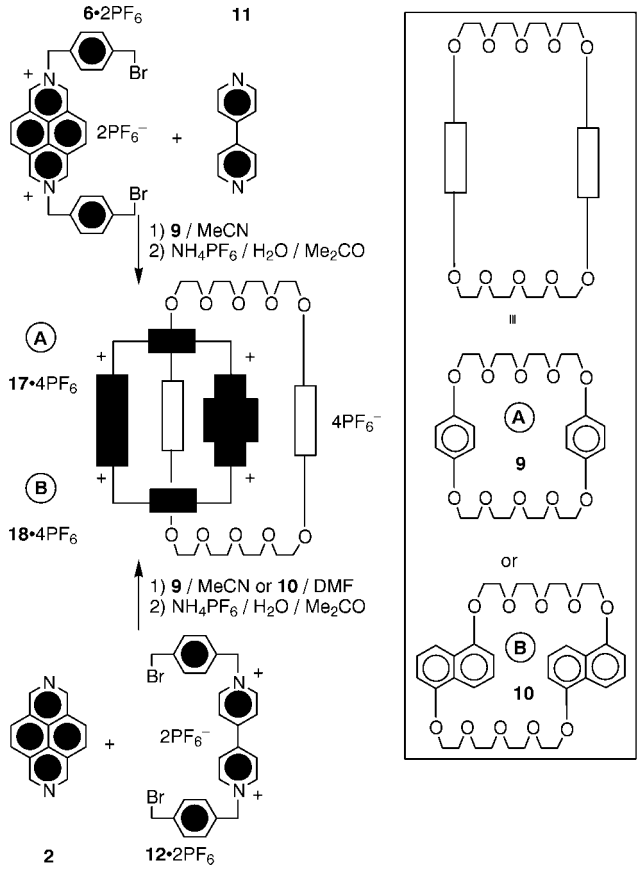

Scheme 5 Template-directed synthesis of the diazapyrenium-containing [2]catenanes $\mathbf{17} \cdot 4PF_6$ and $\mathbf{18} \cdot 4PF_6$.

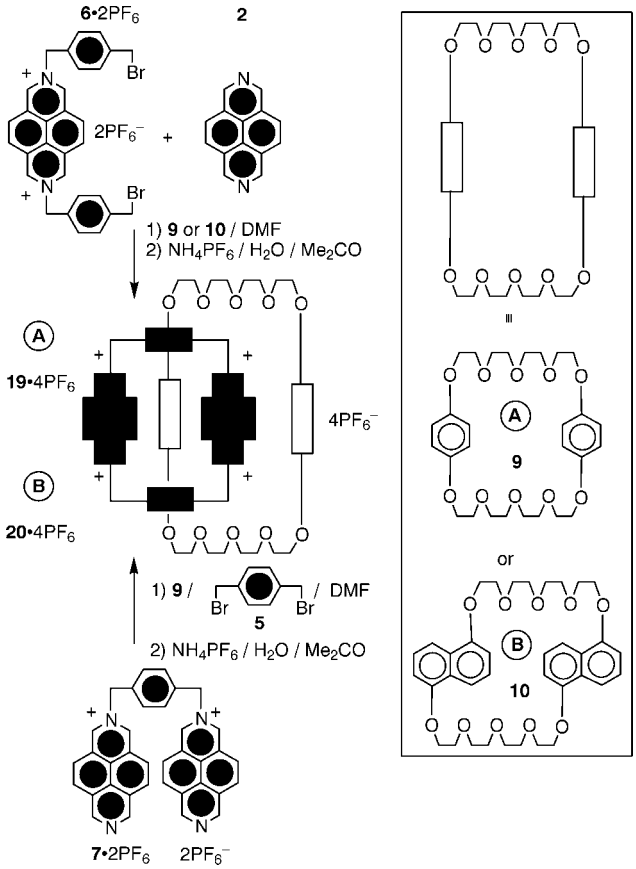

Scheme 6 Template-directed synthesis of the diazapyrenium-containing [2]catenanes $\mathbf{19} \cdot 4PF_6$ and $\mathbf{20} \cdot 4PF_6$.

diazapyrenium-containing [2]rotaxane $\mathbf{30} \cdot 2PF_6$ in a yield of 40%, after counterion exchange.

X-Ray crystallography

The X-ray structural analysis of $[\mathbf{3} \cdot \mathbf{9}] \cdot 2PF_6$ shows [Fig. 1(a) and 1(b)] the guest to be threaded symmetrically through the center of the C_i symmetric macrocyclic cavity with the π-electron deficient dication sandwiched between the π-electron rich 1,4-dioxybenzene rings, each of which exhibit a *syn* relationship for their oxymethylene substituents. The 1 : 1 complex is stabilized further by a pair of [C–H···O] hydrogen bonds between the methyl groups of the guest and the central oxygen atoms of the polyether linkages of the host. A summary of the [π···π] stacking and [C–H···O] hydrogen bonding geometries is given in Table 2. Although the 1 : 1

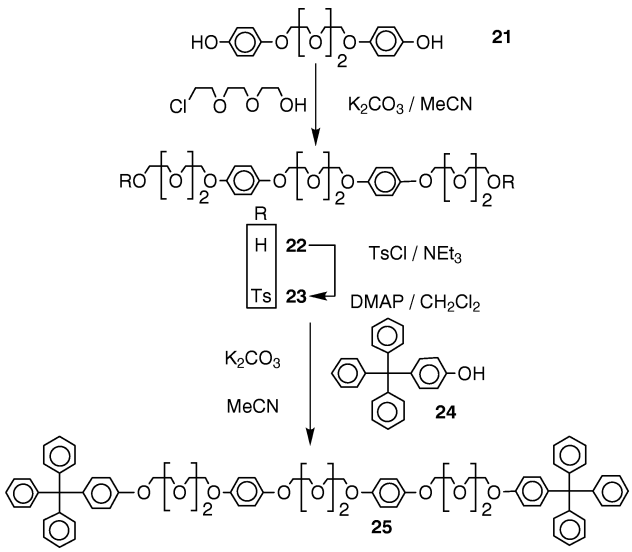

Scheme 7 Synthesis of the dumbbell-shaped compound **25**.

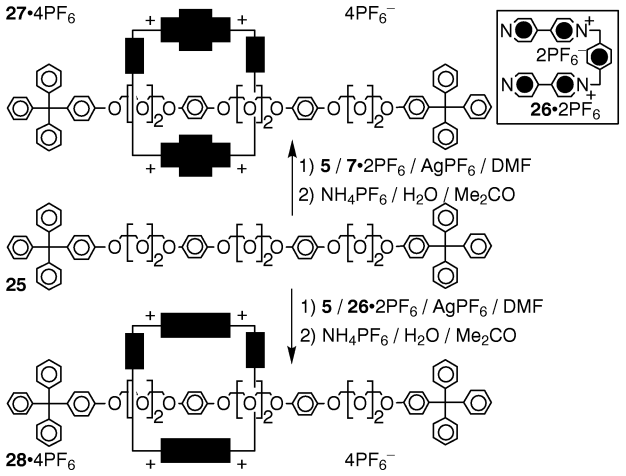

Scheme 8 Template-directed synthesis of the diazapyrenium-containing [2]rotaxanes $\mathbf{27}\cdot 4PF_6$ and $\mathbf{28}\cdot PF_6$.

complexes pack to form stacks [Fig. 1(c)] that extend in the crystallographic *a* direction, there is no [π···π] overlap between adjacent 1,4-dioxybenzene rings but there are pairs of intercomplex [C–H···π] interactions between diametrically opposite β-methylene groups in one complex and the 1,4-dioxybenzene rings in adjacent complexes, the [H···π] distance being 2.72 Å and the [C–H···π] angle 138°.

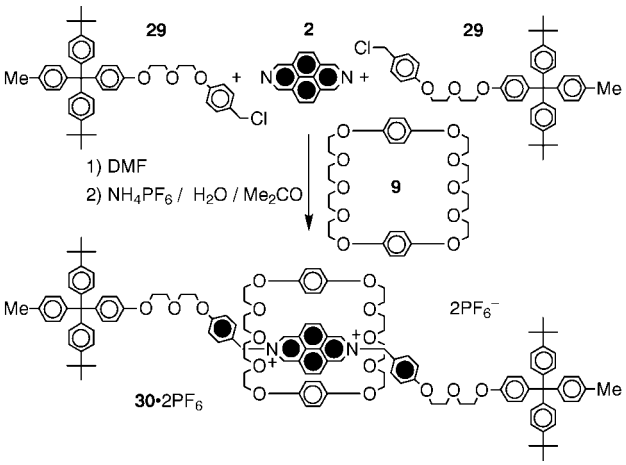

Scheme 9 Template-directed synthesis of the diazapyrenium-containing [2]rotaxane $\mathbf{30}\cdot 2PF_6$.

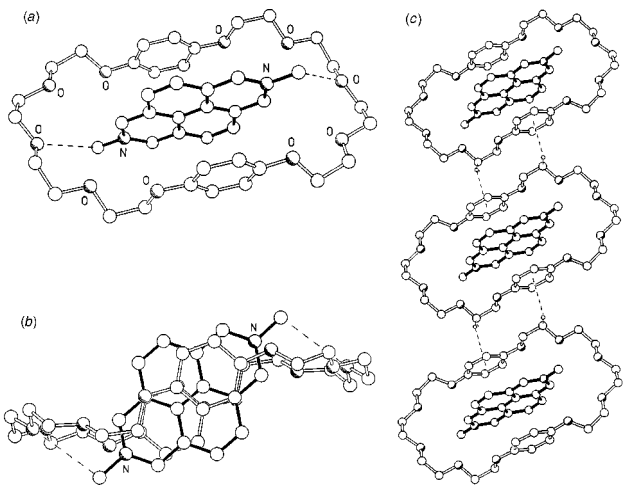

Fig. 1 Ball-and-stick representations [(*a*) and (*b*)] of the geometry adopted by $[\mathbf{3}\cdot\mathbf{9}]^{2+}$ in the solid state and (*c*) one of the polar stacks formed by $[\mathbf{3}\cdot\mathbf{9}]^{2+}$ in the crystal. The dashed lines in (*a*) and (*b*) indicate intracomplex [C–H···O] hydrogen bonds. The dashed lines in (*c*) indicate intercomplex [C–H···π] interactions.

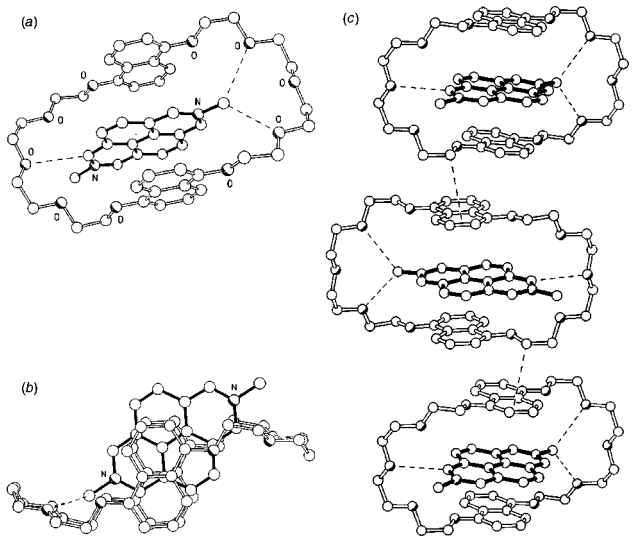

Fig. 2 Ball-and-stick representations [(*a*) and (*b*)] of the geometry adopted by $[\mathbf{3}\cdot\mathbf{10}]^{2+}$ in the solid state and (*c*) one of the polar stacks formed by $[\mathbf{3}\cdot\mathbf{10}]^{2+}$ in the crystal. The dashed lines in (*a*) and (*b*) indicate intracomplex [C–H···O] hydrogen bonds. The dashed lines in (*c*) indicate intercomplex [C–H···π] interactions in addition to the [C–H···O] hydrogen bonds.

The solid state superstructure of $[\mathbf{3}\cdot\mathbf{10}]\cdot 2PF_6$ shows (Fig. 2) a co-conformation[8] that differs markedly from $[\mathbf{3}\cdot\mathbf{9}]\cdot 2PF_6$. The host has approximate molecular C_{2h} symmetry about an axis passing through the centers of the two naphthalene rings [Fig. 2(b)], the two polyether linkages having classical all-*gauche* conformations. However, the guest is not positioned centrosymmetrically within the cavity of the host; it is displaced both vertically and laterally [Fig. 2(b)] with respect to the center of the macroring cavity. Despite this offset, there is still appreciable overlap and hence [π···π] stabilization between the π-electron rich naphthalene rings and the π-electron deficient diazapyrene unit. Secondary stabilization is achieved [Fig. 2(a)] by [C–H···O] hydrogen bonding between one of the methyl groups on the guest and the second and fourth polyether oxygen atoms of one linkage and between one of the α-CH hydrogen atoms and the central oxygen atom in the other. The absence of dibenzyl substituents (*vide infra*) again permits the formation of stacked arrays in the solid state [Fig. 2(c)] comparable with those present in $[\mathbf{3}\cdot\mathbf{9}]\cdot 2PF_6$ but, in this case, involving partial overlap between the naphthalene rings of adjacent complexes. The mean intercomplex interplanar separation is 3.41 Å. Supplementing this weak interaction, there is an intercomplex [C–H···π] interaction between one of the oxymethylene groups in one molecule and the center of one of the fused benzene rings of the 1,5-dioxynaphthalene residue of another. The [H···π] distance is 2.63 Å and the [C–H···π] angle is 153°.

The X-ray crystallographic investigation of $[\mathbf{4}\cdot\mathbf{9}]\cdot 2PF_6$ revealed [Fig. 3(a) and 3(b)] the macrocycle to have the normal open-box like geometry through which is threaded the guest in a centrosymmetric manner. The diazapyrenium core is positioned centrally (Table 2) between the two π-electron rich 1,4-dioxybenzene rings, which have their pairs of oxymethylene substituents displaying *anti* geometries in this solid state superstructure. The guest, which has its benzyl groups in an open-book conformation with respect to the diazapyrenium unit, has its [N···N] axis more steeply inclined [Fig. 3(b) and Table 2] to the mean plane of the host than in the $[\mathbf{3}\cdot\mathbf{9}]\cdot 2PF_6$ complex. In addition to the [π···π] stabilizing interactions between the diazapyrenium unit and the 1,4-dioxybenzene rings of the host in the complex, there are pairs of [C–H···O] hydrogen bonds between both the α-diazapyrenium hydrogen atoms and one of each of the pair of

Table 2 Distances (Å) and angles (°) characterizing the [2]pseudorotaxanes $[\mathbf{3}\cdot\mathbf{9}]\cdot 2PF_6$, $[\mathbf{3}\cdot\mathbf{10}]\cdot 2PF_6$, $[\mathbf{4}\cdot\mathbf{9}]\cdot 2PF_6$, and $[\mathbf{4}\cdot\mathbf{10}]\cdot 2PF_6$, the tetracationic cyclophane $\mathbf{14}\cdot 4PF_6$ and the [2] catenanes $\mathbf{17}\cdot 4PF_6$ and $\mathbf{19}\cdot 4PF_6$

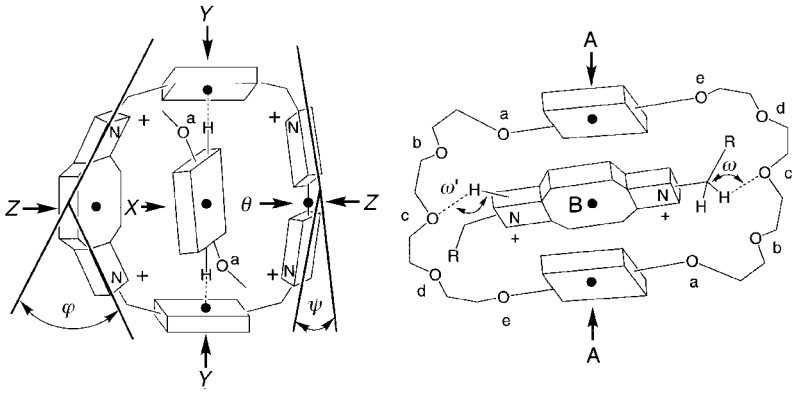

Compound	θ^a	ψ^b	φ^c	τ^d	[Y···Y]^e	[Z···Z]^f	[X···Y]^g	[H···Y]^h	[X–H···Y]^i	[Z···X]^j	[A···A]^k	[A···B]^l	[C–H···O]^m	[C···O]^n	[H···O]^o
$[\mathbf{3}\cdot\mathbf{9}]\cdot 2PF_6$	—	—	—	21	—	—	—	—	—	—	6.90	3.45	159	3.43	2.54
$[\mathbf{3}\cdot\mathbf{10}]\cdot 2PF_6$	—	—	—	8	—	—	—	—	—	—	6.84	3.44	160	3.22	2.30
												3.40	131	3.15	2.43
													160	3.21	2.30
$[\mathbf{4}\cdot\mathbf{9}]\cdot 2PF_6$	—	—	—	45	—	—	—	—	—	—	7.10	3.54	160	3.36	2.44
													147	3.31	2.46
$[\mathbf{4}\cdot\mathbf{10}]\cdot 2PF_6$	—	—	—	39	—	—	—	—	—	—	6.96	3.48	176	3.33	2.35
$\mathbf{14}\cdot 4PF_6$	17	19	15	—	10.37	6.55	—	—	—	—	—	—	—	—	—
$\mathbf{17}\cdot 4PF_6{}^p$	17	27	26	49	10.13	7.02	5.07	2.79	165	3.60	6.77	3.35	164	3.36	2.42
										3.42		3.42			
$\mathbf{19}\cdot 4PF_6{}^p$	—	—	24	48	10.13	6.86	5.07	2.79	162	3.42	6.76	3.44	133	3.03	2.29
			25							3.44		3.32	163	3.31	2.38

[a] Average of the moduli of the four [C–C–C–C] torsional angles about the [C–C] bond linking the pyridinium rings. [b] Angle between the axes of the two $[CH_2–N^+]$ bonds of the bipyridinium unit. [c] Angle between the axes of the two $[CH_2–N^+]$ bonds of the diazapyrenium unit. [d] Angle between the $[O^a\cdots O^a]$ and $[N^+\cdots N^+]$ axes. [e] Separation between the centroids of the *p*-phenylene units of the tetracationic cyclophane. [f] Separation between the centroids of the dicationic units of the tetracationic cyclophane. [g] Separation between the centroid of one the *p*-phenylene units of the tetracationic cyclophane and the centroid of the 'inside' dioxyarene unit. [h] Shortest separation between the centroid of one the *p*-phenylene units and one of the hydrogen atoms of the 'inside' dioxyarene unit. [i] Angle associated with the [C–H···π] interaction. [j] Separation between the centroid of one the dicationic units of the tetracationic cyclophane and the centroid of the 'inside' dioxyarene unit. [k] Interplanar separation between the dioxyarene units. [l] Interplanar separation between the diazapyrenium and one of the dioxyarene units. [m] Angles (ω and ω') associated with the [C–H···O] hydrogen bonds. [n] [C···O] distance associated with the [C–H···O] hydrogen bonds. [o] [H···O] distance associated with the [C–H···O] hydrogen bonds. [p] Although there is a small amount of disorder in the polyether chains in these structures, it does not involve the regions associated with hydrogen bonding, which are clearly resolved.

the benzylic methylene hydrogen atoms in $\mathbf{4}^{2+}$ and the central oxygen atoms of the polyether linkages in the host [Fig. 3(a) and Table 2]. The phenyl rings of the benzyl groups do not enter into any significant intracomplex [C–H···π] interactions with the 1,4-dioxybenzene rings. In contrast with $[\mathbf{3}\cdot\mathbf{9}]\cdot 2PF_6$, in this [2]pseudorotaxane there is no formation of any continuous stack. The conformation of $\mathbf{4}^{2+}$ in the complex is very little changed compared with the conformation in its uncomplexed state. In the complex, the mean torsional twists about the $[CH_2–N^+]$ and the $[CH_2–Ph]$ bonds are 74 and 84°, respectively, *cf.* values of 79 and 90° in $[\mathbf{4}\cdot\mathbf{9}]\cdot 2PF_6$.

The [2]pseudorotaxane $[\mathbf{4}\cdot\mathbf{10}]\cdot 2PF_6$ crystallizes with two crystallographically independent C_i symmetric complexes in the asymmetric unit. Their geometries are, within statistical significance, identical. In common with $[\mathbf{4}\cdot\mathbf{9}]\cdot 2PF_6$, the guest is sandwiched symmetrically (Fig. 4) between the pair of 1,5-dioxynaphthalene rings of the host. This [π···π] stabilization is supplemented by a pair of [C–H···O] hydrogen bonds (Table 2) between a hydrogen atom of each of the benzylic methylene groups on the guest and the central oxygen atoms of each polyether arm of the host. The benzyl substituents of the guest are oriented in an open-book conformation with respect to the diazapyrenium core with $[CH_2–N^+]$ and the $[CH_2–Ph]$ torsion angles of 73 and 87°, respectively, in one independent complex, and 72 and 84° in the other. Thus, the formation of an extended stacked array in the solid state is inhibited in the same way as it is for $[\mathbf{4}\cdot\mathbf{9}]\cdot 2PF_6$, adjacent complexes being orientated orthogonally with respect to each other. No significant intercomplex [π···π], [C–H···π], or [C–H···O] interactions were identified.

The solid state structure of the tetracationic cyclophane $\mathbf{14}\cdot 4PF_6$ reveals [Fig. 5(a)] a conformation that is noticeably modified compared (*vide infra*) to that which is adopted in the [2]catenane $\mathbf{17}\cdot 4PF_6$. The overall dimensions (6.6 × 10.4 Å) show (Table 2) a small increase in the separation of the centroids of the two *p*-xylyl rings and a slightly more marked increase in the separation of the two π-electron deficient components. The most significant change in the conformation is a tilting 'inward' [Fig. 5(b)] of the planes of the diazapyrenium and bipyridinium units with respect to the mean plane of the cyclophane (as defined by the four methylene carbon atoms), and a tilting 'outwards' of the planes of the two *p*-xylyl rings. The diazapyrenium unit is inclined by 58°, the bipyridinium rings by 64 and 81°, and the two *p*-xylyl rings by 66 and 72°, respectively. The twisting (θ) distortion within the cyclophane is unchanged from the [2]catenane $\mathbf{17}\cdot 4PF_6$, but the bowings (ψ and φ) of the two different π-electron deficient units are reduced. An analysis of the packing of the cyclophanes does not reveal any extended [π···π] stacking arrangement. The only proximal relationships are between *p*-xylyl rings of symmetry related molecules for which the [centroid···centroid] separation is 4.10 Å, with the planes of the rings being inclined by 22°. The tetracations do however, form [Fig. 5(c)] polar stacks that extend in the crystallographic *a* direction, forming restricted channels with one of the hexafluorophosphate anions being held between the 'cupped-face' of one molecule and the restricted face of the next one within the stack. The

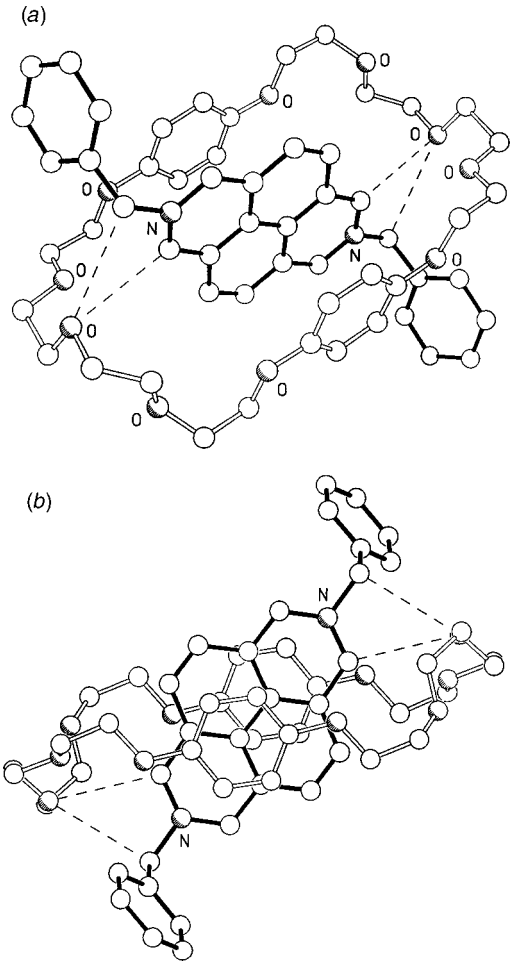

Fig. 3 Ball-and-stick representations [(*a*) and (*b*)] of the geometry adopted by $[\mathbf{4}\cdot\mathbf{9}]^{2+}$ in the solid state. The dashed lines indicate intracomplex [C–H···O] hydrogen bonds.

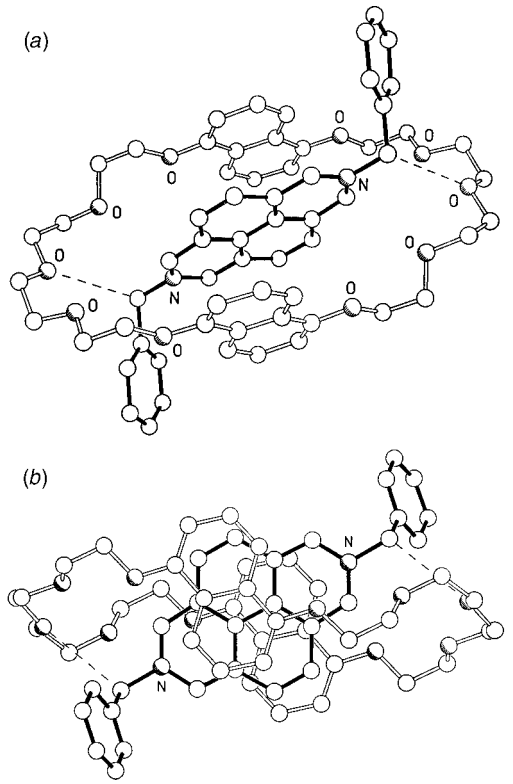

Fig. 4 Ball-and-stick representations [(*a*) and (*b*)] of the geometry adopted by $[\mathbf{4}\cdot\mathbf{10}]^{2+}$ in the solid state. The dashed lines indicate intracomplex [C–H···O] hydrogen bonds.

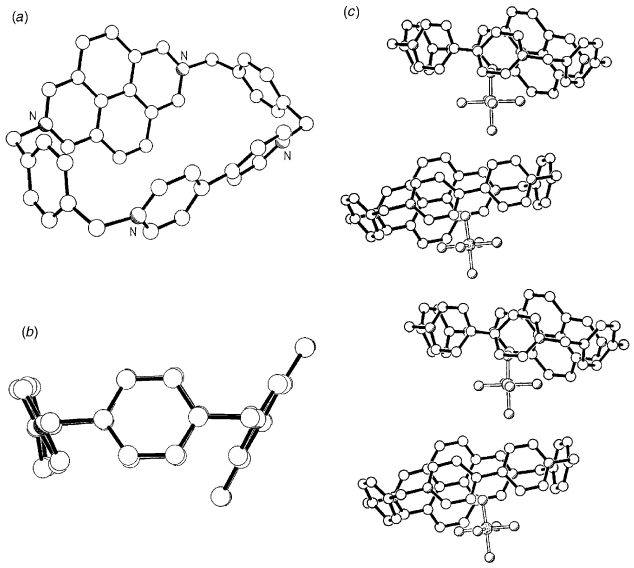

Fig. 5 Ball-and-stick representations [(*a*) and (*b*)] of the geometry adopted by $\mathbf{14}^{4+}$ in the solid state and (*c*) one of the polar stacks formed by $\mathbf{14}^{4+}$ and the hexafluorophosphate anions in the crystal.

intrastack separation of adjacent hexafluorophosphate centers is 7.70 Å.

The solid-state structure of the [2]catenane $\mathbf{17}\cdot 4PF_6$ shows [Fig. 6(a)] the diazapyrenium unit of the tetracationic cyclophane to be positioned within the cavity of the macrocyclic polyether, which adopts a conformation with a C_2 symmetry axis passing through the centers and normal to the planes of the two 1,4-dioxybenzene rings. The $[OC_6H_4O]$ axes of the 'inside' and 'outside' 1,4-dioxybenzene rings are [Fig. 6(b)] inclined with respect to each other (*cf.* a parallel arrangement in $[\mathbf{3}\cdot\mathbf{9}]\cdot 2PF_6$ and $[\mathbf{4}\cdot\mathbf{9}]\cdot 2PF_6$). In addition to the [π···π] stabilization between the π-electron rich 1,4-dioxybenzene rings and the π-electron deficient bipyridinium and diazapyrenium components of the tetracationic cyclophane, there are

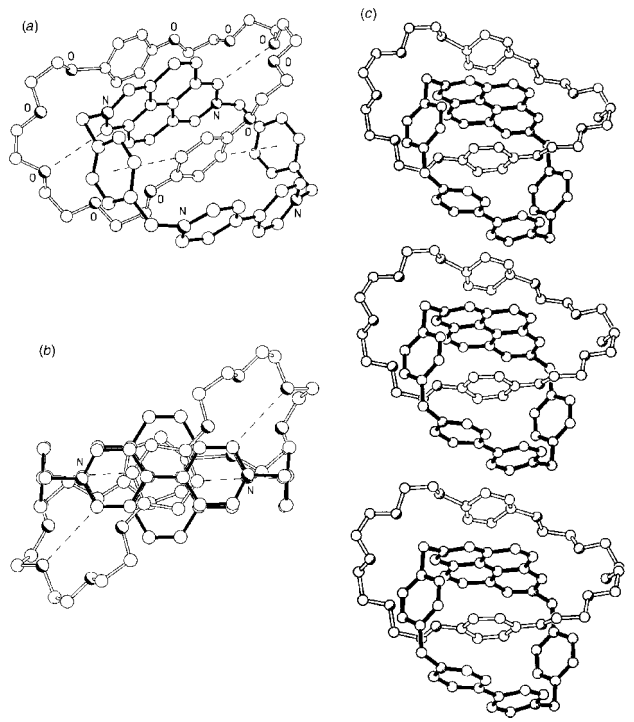

Fig. 6 Ball-and-stick representations [(*a*) and (*b*)] of the geometry adopted by $\mathbf{17}^{4+}$ in the solid state and (*c*) one of the donor/acceptor stacks formed by $\mathbf{17}^{4+}$ in the crystal. The dashed lines in (*a*) and (*b*) indicate intracatenane [C–H···O] and [C–H···π] interactions.

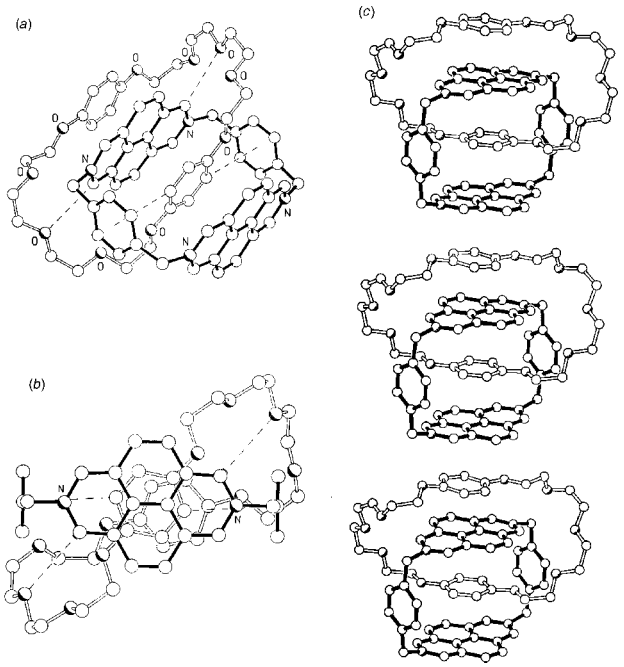

Fig. 7 Ball-and-stick representations [(*a*) and (*b*)] of the geometry adopted by $\mathbf{19}^{4+}$ in the solid state and (*c*) one of the donor/acceptor stacks formed by $\mathbf{19}^{4+}$ in the crystal. The dashed lines in (*a*) and (*b*) indicate intracatenane [C–H···O] and [C–H···π] interactions.

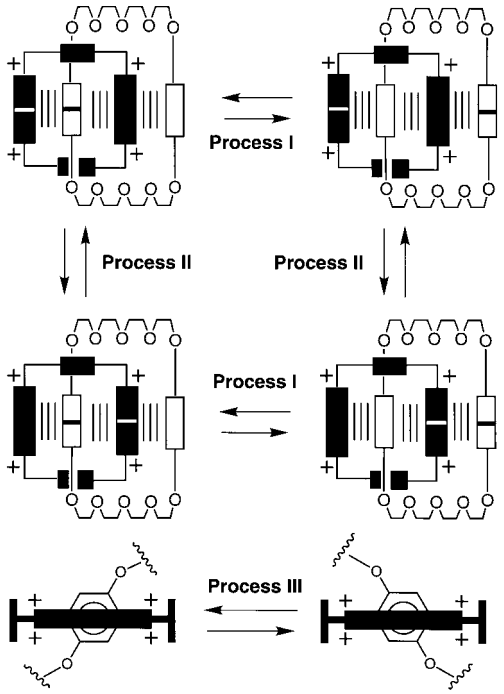

Fig. 8 The dynamic processes I–III associated with the [2]catenanes $\mathbf{17}\cdot 4PF_6$–$\mathbf{20}\cdot 4PF_6$ in solution.

(Table 2) [C–H···O] hydrogen bonds between α-diazapyrenium hydrogen atoms and the central oxygen atoms of each polyether linkage. There are also [C–H···π] interactions between a diametrically opposite pair of inside 1,4-dioxybenzene hydrogen atoms and the *p*-xylyl spacers in the tetracationic cyclophane. A notable feature of the crystal structure is the existence of disorder (lateral slippage) in the positioning of the outside 1,4-dioxybenzene ring and its associated polyether linkages. Despite this disorder, there is still a retention of an interplanar separation between this disordered ring and the inside diazapyrenium unit of 3.35 Å, compatible with the maintenance of [π···π] stabilization. Inspection of the packing of the [2]catenane molecules in the solid state reveals [Fig. 6(c)] a familiar polar stacking motif with the outside 1,4-dioxybenzene rings of one complex positioned in a [π···π] stacking arrangement with respect to the outside bipyridinium unit of the next (interplanar separation 3.52 Å).

The single crystal structural analysis of the [2]catenane $\mathbf{19}\cdot 4PF_6$ reveals [Fig. 7(a)] an arrangement that is very similar to that observed for the closely related $\mathbf{17}\cdot 4PF_6$. One of the π-electron rich 1,4-dioxybenzene rings is sandwiched between the two π-electron deficient diazapyrenium units with [centroid···centroid] separations that are virtually unchanged from those in $\mathbf{17}\cdot 4PF_6$. The complex is further stabilized (Table 2) by (*i*) [C–H···π] interactions between hydrogen atoms on the *ortho* positions of the 1,4-dioxybenzene ring and the *p*-xylyl rings of the tetracationic cyclophane, and (*ii*) [C–H···O] hydrogen bonds between the α-diazapyrenium hydrogen atoms and the central oxygen atoms of the polyether linkages within the macrocyclic polyether. In common with $\mathbf{17}\cdot 4PF_6$, there is disorder in the positioning of the outside 1,4-dioxybenzene ring with respect to the crystallographically imposed molecular C_2 axis, the 1,4-dioxybenzene ring being slid laterally [Fig. 7(b)] but parallel to the plane of the diazapyrenium unit. As in $\mathbf{17}\cdot 4PF_6$, there is [Fig. 7(c)] formation of polar donor/acceptor stacks, the only significant difference being that, in the lattice of $\mathbf{19}\cdot 4PF_6$, the 'outside' 1,4-dioxybenzene ring is sandwiched between *two* diazapyrenium units as opposed to one diazapyrenium and one bipyridinium unit. The interstack donor/acceptor separation is

Table 3 Kinetic parameters for the dynamic processes associated with the [2]catenanes $\mathbf{17}\cdot 4PF_6$–$\mathbf{20}\cdot 4PF_6$ and with the [2]rotaxanes $\mathbf{27}\cdot 4PF_6$ and $\mathbf{28}\cdot 4PF_6$ in solution

Compound	Probe protons	Solvent	$\Delta\nu$/Hz	k/s^{-1}	T/K	$\Delta G\ddagger$/kcal mol^{-1}	Process
$\mathbf{17}\cdot 4PF_6$	'Outside' [OC_6H_4O]	CD_3CN	10	40	355	18.5	I[a]
	'Inside' [OC_6H_4O]	CD_3CN	10	40	355	18.5	I[a]
	[CH_2N^+]	$(CD_3)_2CO$	50	110	212	10.3	III[b,c]
$\mathbf{18}\cdot 4PF_6$	α-Bipyridinium	CD_3CN	6	10	355	19.1	I[b]
	β-Bipyridinium	CD_3CN	6	10	355	19.1	I[a]
$\mathbf{19}\cdot 4PF_6$	'Outside' [OC_6H_4O]	CD_3CN	1	3	369	20.8	I[a]
	α-Diazapyrenium	CD_3CN	12	30	280	14.5	II[b]
	'Inside' α-diazapyrenium	$(CD_3)_2CO$	151	340	219	10.2	III[b]
	'Outside' α-diazapyrenium	$(CD_3)_2CO$	64	140	205	9.8	III[b]
$\mathbf{20}\cdot 4PF_6$	α-Diazapyrenium	CD_3CN	10	20	296	15.5	IV[b]
	α-Diazapyrenium	CD_3CN	162	360	322	15.2	IV[b]
$\mathbf{27}\cdot 4PF_6$	α-Diazapyrenium	CD_3CN	15	30	350	18.1	V[b]
	α-Diazapyrenium	CD_3CN	192	430	210	9.6	III[b]
$\mathbf{28}\cdot 4PF_6$	α-Bipyridinium	CD_3CN	86	190	274	13.1	V[b]

[a] The exchange method was employed to determine the kinetic parameters (error for $k \pm 5$ s^{-1}, error for $\Delta G\ddagger \pm 0.2$ kcal mol^{-1}). [b] The coalescence method was employed to determine the kinetic parameters. [c] Determined for the major translational isomer.

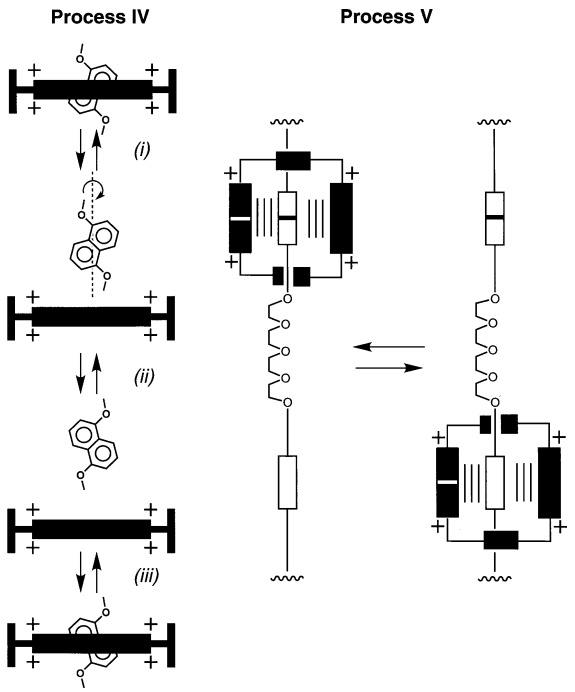

Fig. 9 The dynamic process IV associated with the [2]catenanes **18** · $4PF_6$ and **20** · $4PF_6$ in solution and the dynamic process V associated with the [2]rotaxanes **27** · $4PF_6$ and **28** · $4PF_6$ in solution.

noticeably reduced from 3.52 Å in **17** · $4PF_6$ to 3.37 Å in **19** · $4PF_6$, reflecting the stronger interaction of the diazapyrenium unit over the bipyridinium unit.

^{1}H NMR spectroscopy

In the [2]catenanes **17** · $4PF_6$–**20** · $4PF_6$, the dynamic processes I–IV can occur (Table 3 and Fig. 8 and 9) in solution. Process I corresponds to the circumrotation of the macrocyclic polyether through the cavity of the tetracationic cyclophane. Process II involves the circumrotation of the tetracationic cyclophane through the cavity of the macrocyclic polyether. Process III corresponds to the 'rocking' of the [O···O] axis of the 'inside' 1,4-dioxybenzene unit with respect to the mean plane of the tetracationic cyclophane. Process IV involves (*i*) dislodgment of the 1,5-dioxynaphthalene unit from the cavity of the tetracationic cyclophane, (*ii*) its 180° rotation around the [O···O] axis, and (*iii*) its reinsertion inside the cavity of the tetracationic cyclophane. In the [2]rotaxanes **27** · $4PF_6$ and **28** · $4PF_6$, the dynamic processes III and V can occur in solution. Process V corresponds to the 'shuttling' of the tetracationic cyclophane from one 1,4-dioxybenzene unit to the other.

In **17** · $4PF_6$, process I is slow on the ^{1}H NMR timescale at 300 K in CD_3CN. As a result, the protons attached to the 1,4-dioxybenzene units located inside and outside the cavity of the tetracationic cyclophane component give rise to two sets of

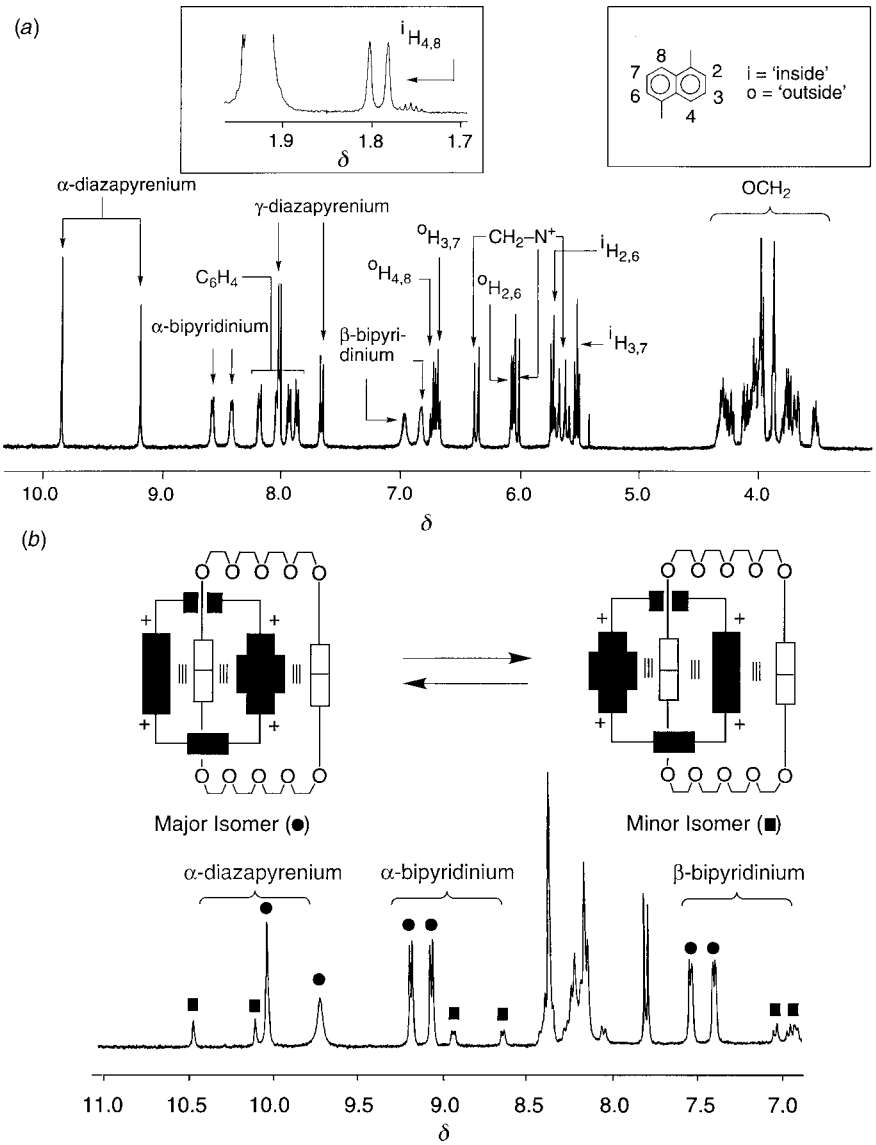

Fig. 10 Partial ^{1}H NMR (400 MHz) spectra of the [2]catenane **18** · $4PF_6$ (*a*) in CD_3CN at 333 K and (*b*) in $(CD_3)_2CO$ at 253 K.

signals at δ 2.63 and 5.16, respectively. Upon warming the solution, broadening of these signals is observed as process I becomes faster. Saturation transfer experiments, performed by irradiating either the 'inside' or the 'outside' 1,4-dioxybenzene protons, indicated that the two sets of protons are in exchange. Line broadening analysis[9] revealed a free energy barrier of 18.5 kcal mol^{-1} at 355 K for process I. At 193 K in $(CD_3)_2CO$, process II is slow and the signals of two translational isomers can be distinguished in a ratio of 96 : 4. In the major isomer, the diazapyrenium unit resides inside the cavity of the macrocyclic polyether while it is positioned 'outside' in the minor isomer. At this temperature, process III is also slow and, as a result, the 'inside' and 'outside' [CH_2N^+] protons of each isomer give rise to two AB systems. On warming the solution, coalescence of the two AB systems into two singlets is observed. By employing the approximate coalescence treatment,[10] a free energy barrier of 10.3 kcal mol^{-1} at a coalescence temperature of 212 K was determined for process III in the case of the major isomer.

In the ^1H NMR spectrum of a CD_3CN solution of **18**·$4PF_6$ recorded at 333 K, the resonances associated with the 'inside' and 'outside' 1,5-dioxynaphthelene units can be distinguished [Fig. 10(a)] indicating that process I is slow on the ^1H NMR timescale. Furthermore, two sets of signals are observed for the α-diazapyrenium, as well as for the α-bipyridinium, protons as a result of the local C_2 symmetry imposed by the 'inside' 1,5-dioxynaphthalene unit. On warming the solution to 355 K, broadening of these signals is observed, as process I becomes faster. Saturation transfer experiments, performed by irradiating either the 'inside' or the 'outside' 1,5-dioxynaphthalene protons, indicated that these protons are in exchange. Line broadening analysis[9] revealed a free energy barrier of 19.1 kcal mol^{-1} at 355 K for process I. On cooling a $(CD_3)_2CO$ solution of **18**·$4PF_6$ to 253 K, process II becomes slow on the ^1H NMR timescale and the signals of two translational isomers can be distinguished [Fig. 10(b)] in a ratio of 82 : 18. In the major isomer, the diazapyrenium unit resides inside the cavity of the macrocyclic polyether, while it is positioned outside in the minor isomer.

In **19**·$4PF_6$, process I is slow on the ^1H NMR timescale at 300 K in CD_3CN. As a result, the 'inside' and 'outside' 1,4-dioxybenzene protons give rise to two sets of signals at δ 1.90 and 5.19, respectively. Upon warming the solution, broadening of these signals is observed, as process I becomes faster. Saturation transfer experiments, performed by irradiating either the 'inside' or the 'outside' 1,4-dioxybenzene protons, indicated that the two sets of protons are in exchange. Line broadening analysis[9] revealed a free energy barrier of 20.8 kcal mol^{-1} at 369 K for process I. At 300 K, process II is fast on the ^1H NMR timescale in $(CD_3)_2CO$ and only one singlet is observed [Fig. 11(a)] for the α-diazapyrenium protons. On cooling the solution, this singlet broadens [Fig. 11(b) and 11(c)] and separates [Fig. 11(d)] into two singlets at 273 K, as process II becomes slow. By employing the coalescence treatment,[10] a free energy barrier of 14.5 kcal mol^{-1} at a coalescence temperature of 280 K was determined for process II. On further cooling, the two singlets associated with the 'inside' and 'outside' α-diazapyrenium protons separate into four singlets as process III becomes slow. By employing the coalescence treatment,[10] free energy barriers of 10.2 and 9.8 kcal mol^{-1} at coalescence temperatures of 219 and 205 K, respectively, were determined for process III.

In the ^1H NMR spectrum of a CD_3CN solution of **20**·$4PF_6$ recorded at 333 K, the resonances associated with the 'inside' and 'outside' 1,5-dioxynaphthelene units can be distinguished indicating that process I is slow on the ^1H NMR timescale. Furthermore, two singlets are observed for the α-diazapyrenium protons as a result of the local C_2 symmetry imposed by the 'inside' 1,5-dioxynaphthalene unit. On warming the solution to 355 K, these two singlets coalesce into only one, as process IV becomes faster. By employing the coalescence treatment,[10] free energy barriers of 15.5 and 15.2 kcal mol^{-1} at coalescence temperatures of 296 and 322 K, respectively, were determined for process IV.

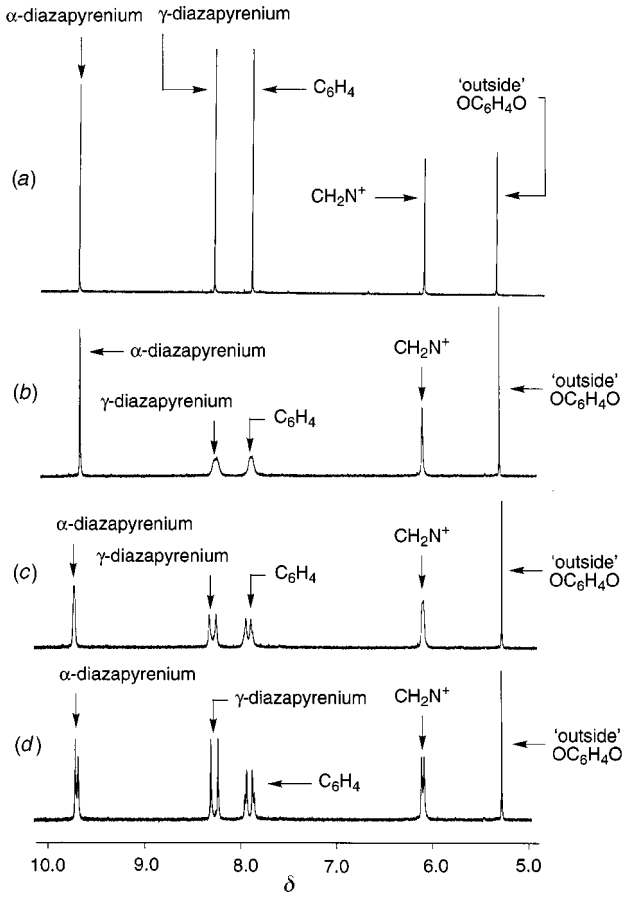

Fig. 11 Partial ^1H NMR (400 MHz) spectra of the [2]catenane **19**·$4PF_6$ in $(CD_3)_2CO$ at (*a*) 300, (*b*) 293, (*c*) 283 and (*d*) 273 K.

In **27**·$4PF_6$, process V is slow on the ^1H NMR timescale at 300 K in CD_3CN and the α-diazapyrenium protons give rise [Fig. 12(b)] to two singlets. On warming the solution, coalescence of the two singlets into only one occurs [Fig.

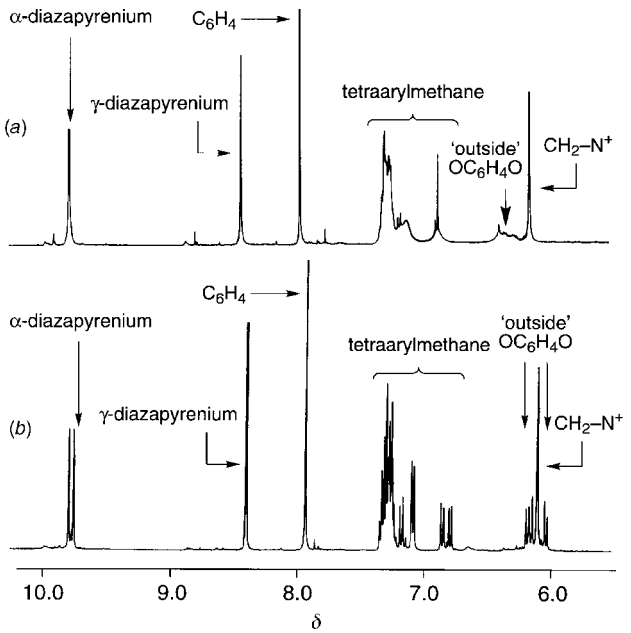

Fig. 12 Partial ^1H NMR (400 MHz) spectra of the [2]rotaxane **27**·$4PF_6$ in CD_3CN at (*a*) 333, and (*b*) 300 K.

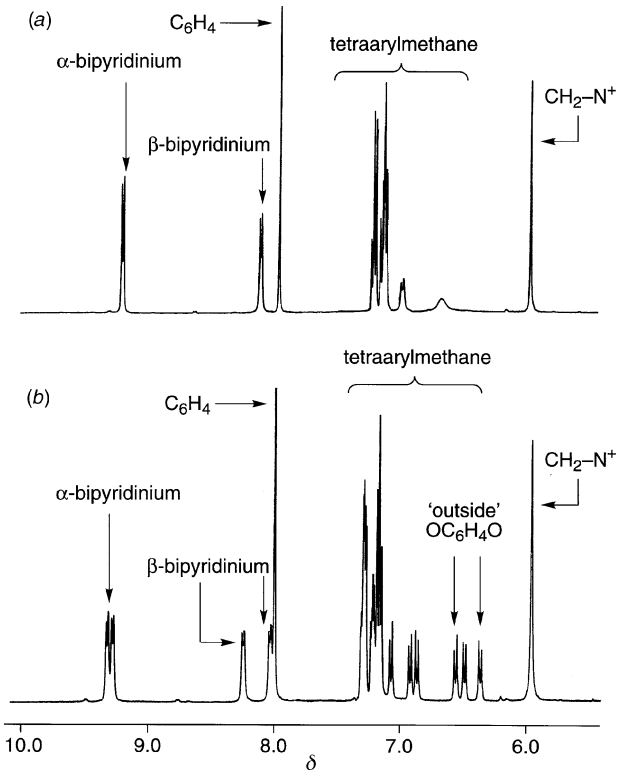

Fig. 13 Partial ^{1}H NMR (400 MHz) spectra of the [2]rotaxane **28** · 4PF_6 in $(CD_3)_2CO$ at (*a*) 300, and (*b*) 243 K.

12(a)], as process V becomes faster. By employing the coalescence treatment,[10] a free energy barrier of 18.1 kcal mol^{-1} at a coalescence temperature of 350 K was determined for process V. At 193 K in $(CD_3)_2CO$, the α-diazapyrenium protons give rise to four singlets, as process III is slow. On warming the solution, coalescence of these four singlets into two occurs, as process III becomes faster. By employing the coalescence treatment,[10] a free energy barrier of 9.6 kcal mol^{-1} at a coalescence temperature of 210 K was determined for process III.

In **28** · 4PF_6, process V is slow on the ^{1}H NMR timescale at 243 K in $(CD_3)_2CO$ and the α-bipyridinium protons give rise [Fig. 13(b)] to two sets of signals. On warming the solution, coalescence of the two sets of signals into only one occurs [Fig. 13(a)], as process V becomes faster. By employing the coalescence treatment,[10] a free energy barrier of 13.2 kcal mol^{-1} at a coalescence temperature of 274 K was determined for process V.

Previous studies have demonstrated[11] that the passage of the macrocyclic polyether **9** over 4-[bis(4-*tert*-butylphenyl)-4-methylphenylmethyl]phenyl-based stoppers can occur at elevated temperatures. Indeed, the [2]rotaxane **30** · 2PF_6 dissociates into its separate dumbbell-shaped and macrocyclic components when heated at 100 °C in $(CD_3)_2SO$. The process can be monitored by ^{1}H NMR spectroscopy following the changes in the intensities of the resonances associated with the diazapyrenium protons of the [2]rotaxane relative to those of the 'free' dumbbell-shaped compound. However, since signals associated with products of the degradation of the dumbbell-shaped component appear after *ca.* 100 min, the dissociation process could not be followed clearly to completion.

Conclusions

Diazapyrenium-containing guests are bound by dioxyarene-based polyether hosts as a result of [C–H···O] hydrogen bonds and [π···π] stacking interactions. The corresponding [2]pseudorotaxanes are significantly more stable than the bipyridinium-based analogs. This recognition motif has been exploited to synthesize [2]catenanes and [2]rotaxanes incorporating one or two diazapyrenium recognition sites in one of their two mechanically interlocked components. In the case of two [2]catenanes, a tetracationic cyclophane incorporating one diazapyrenium and one bipyridinium recognition site was mechanically interlocked with either 1,4-dioxybenzene- or 1,5-dioxynaphthalene-based macrocyclic polyethers. Both [2]catenanes exist as mixtures of two translational isomers in solution. In both instances, the major isomer is the one which incorporates the diazapyrenium recognition site inside the cavity of the macrocyclic polyether component and the bipyridinium one 'outside'. Consistently, the major isomer detected in solution is observed exclusively in the solid state. These results reflect the ability of dioxyarene recognition sites to sustain non-covalent bonding interactions with diazapyrenium recognition sites which are significantly stronger than those achieved with bipyridinium ones. As a result, in the [2]catenanes, the free energy barriers associated with the circumrotation of one macrocyclic component through the cavity of the other and *vice versa* increase significantly on replacing bipyridinium with diazapyrenium recognition sites in the tetracationic cyclophane component.

Experimental

General methods

Chemicals were purchased from Aldrich and used as received. Solvents were purified according to literature procedures.[12] The compounds **9**,[13] [**8**·**9**] · 2PF_6,[5] [**8**·**10**] · 2PF_6,[6] **10**,[5] **12** · 2PF_6,[11] **13**,[13] **15**,[14] **21**,[13] **24**,[11] **26** · 2PF_6,[13] and **29**[11] were prepared following literature procedures. Reactions under high pressure conditions were carried out in Teflon vessels using a custom-built high pressure apparatus manufactured by PSIKA Pressure Systems Limited of Glossop, UK. Thin-layer chromatography (TLC) was carried out using aluminium or plastic plates, coated with Merck 5735 Kieselgel 60F. The developed plates were dried and scrutinized under a UV lamp. Column chromatography was performed using Kieselgel 60 (0.040–0.063 mm mesh, Merck 9385). Melting points were determined with an Electrothermal 9200 melting point apparatus and are uncorrected. Liquid secondary ion mass spectra (LSIMS) were recorded in the positive-ion mode at a scan speed of 5 s per decade on a VG–Zab Spec mass spectrometer (accelerating voltage, 8 keV; resolution, 2000). High resolution liquid secondary ion mass spectra (HRLSIMS) were obtained from a VG–Zab Spec triple-focusing mass spectrometer operating at a resolution of 5000 and using voltage scanning with CsI as a reference. ^{1}H NMR spectra were recorded on a Bruker AC300 (300 MHz) or Bruker AMX400 (400 MHz) spectrometer using the deuterated solvent as lock and residual solvent or tetramethylsilane as internal reference. ^{13}C NMR spectra were recorded on a Bruker AC300 (75.5 MHz) or AMX400 (100 MHz) spectrometer using the JMOD pulse sequence in most cases.

2,7-Diazapyrene (2)

A mixture of **1** (6.35 g, 24 mmol) and aqueous $MeNH_2$ (40%, 60 mL) was stirred for 5 min at ambient temperature and the solvent was removed under reduced pressure. $PhNO_2$ (50 mL) was added to the solid residue and the mixture was heated until a color change was observed. After cooling to ambient temperature, the mixture was filtered off, washed with H_2O (1 × 20 mL), and with Me_2CO (1 × 50 mL). The resulting 1,4,5,8-naphthalenediimide was isolated (6.70 g, 96%)

as a pink powder (mp > 300 °C; LSIMS: *m/z* 294 $[M]^+$). Reduction of this diimide (9.5 g, 72%) and aromatization of the resulting 1,3,6,8-tetrahydro-2,7-diazapyrene were performed as described in the literature[4] to give **2** (2.90 g, 67%) as yellow needles, after crystallization from benzene. mp = 283–285 °C; EIMS: *m/z* 204 $[M]^+$; ^{1}H NMR ($CDCl_3$): δ 8.21 (4H, s), 9.51 (4H, s).

2,7-Dimethyldiazapyrenium bis(hexafluorophosphate) (3·2PF$_6$)

A mixture of **2** (225 mg, 1.10 mmol) and MeI (390 mg, 2.75 mmol) in Me_2SO (25 mL) was stirred for 1 h at 60 °C under an atmosphere of N_2. An orange precipitate appeared after the addition of more MeI (600 mg, 4.23 mmol). The solid was filtered off and dissolved in H_2O–Me_2CO (1:1, 20 mL). Addition of NH_4PF_6 (1.5 g), followed by the evaporation of Me_2CO, caused the appearance of a precipitate which was filtered off and crystallized from MeCN–Pr^i_2O to give **3**·2PF$_6$ (528 mg, 92%) as a yellow powder. mp > 300 °C; LSIMS: *m/z* = 379 $[M - PF_6]^+$, 234 $[M - 2PF_6]^+$; ^{1}H NMR (CD_3CN): δ 4.85 (6H, s), 8.82 (4H, s), 9.81 (4H, s).

2,7-Dibenzyldiazapyrenium bis(hexafluorophosphate) (4·2PF$_6$)

A mixture of **2** (225 mg, 1.10 mmol) and $PhCH_2Br$ (2 mL) in Me_2SO (10 mL) was stirred for 12 h at 60 °C under an atmosphere of N_2. The resulting precipitate was filtered off and dissolved in H_2O–Me_2CO (1:1, 20 mL). Addition of NH_4PF_6 (1.5 g), followed by the evaporation of Me_2CO, caused the appearance of a precipitate which was filtered off and crystallized from MeCN–Pr^i_2O to give **4**·2PF$_6$ (232 mg, 95%) as a yellow solid. mp = 282 °C (decomp.); LSIMS: *m/z* 531 $[M - PF_6]^+$, 386 $[M - 2PF_6]^+$; ^{1}H NMR (CD_3CN): δ 6.25 (4H, s), 7.51–7.55 (6H, m), 7.62–7.67 (4H, m), 8.81 (4H, s), 9.93 (4H, s).

General method for the preparation of the [2]pseudorotaxanes

Equimolar amounts (*ca.* 5 mM) of the host and guest components were dissolved in CD_3CN and a color change was observed immediately. [**3**·**9**]·2PF$_6$: LSIMS: *m/z* 915 $[M - PF_6]^+$; HRLSIMS: *m/z* calc. for $[M - PF_6]^+$ ($C_{44}H_{54}F_6N_2O_{10}P$): 915.3420, found: 915.3388; ^{1}H NMR (CD_3CN): δ 3.62 (16H, m), 3.79 (8H, m), 3.86 (8H, m), 4.91 (6H, s), 5.61 (8H, s), 8.56 (4H, s), 9.75 (4H, s); ^{13}C NMR (CD_3CN): δ 51.0, 68.6, 70.6, 71.5, 71.6, 114.6, 129.5, 130.7, 143.1, 152.2. Crystals of [**3**·**9**]·2PF$_6$, suitable for X-ray structural analysis, were grown by vapor diffusion of Pr^i_2O into a 1:1 solution of **3**·2PF$_6$ and **9** in MeCN. [**3**·**10**]·2PF$_6$: LSIMS: *m/z* 1015 $[M - PF_6]^+$, 870 $[M - 2PF_6]^+$; HRLSIMS: *m/z* calc. for $[M - PF_6]^+$ ($C_{52}H_{58}F_6N_2O_{10}P$): 1015.3733, found: 1015.3718; ^{1}H NMR (CD_3CN): δ 3.75 (8H, m), 3.84 (8H, m), 3.90 (8H, m), 3.97 (8H, m), 4.87 (6H, s), 6.07 (4H, m), 6.55 (8H, m), 8.56 (4H, s), 9.75 (4H, s); ^{13}C NMR (CD_3CN): δ 50.9, 68.7, 70.5, 71.8, 71.8, 105.3, 113.5, 124.9, 125.5, 128.8, 130.0, 141.9, 153.5. Crystals of [**3**·**10**]·2PF$_6$, suitable for X-ray structural analysis, were grown by vapor diffusion of Pr^i_2O into a 1:1 solution of **3**·2PF$_6$ and **10** in MeCN. [**4**·**9**]·2PF$_6$: LSIMS: *m/z* 1067 $[M - PF_6]^+$; HRLSIMS: *m/z* calc. for $[M - PF_6]^+$ ($C_{56}H_{62}F_6N_2O_{10}P$) 1067.4046, found: 1067.4081; ^{1}H NMR (CD_3CN): δ 3.26–3.33 (8H, m), 3.58–3.64 (8H, m), 3.74–3.79 (8H, m), 3.80–3.85 (8H, m), 5.45 (8H, s), 6.36 (4H, s), 7.50–7.62 (6H, m), 7.78–7.85 (4H, m), 8.53 (4H, s), 9.85 (4H, s); ^{13}C NMR (CD_3CN): δ 67.4, 68.4, 70.6, 71.3, 71.5, 114.5, 130.2, 130.6, 131.0, 131.2, 134.5, 142.2, 152.0. Crystals of [**4**·**9**]·2PF$_6$, suitable for X-ray structural analysis, were grown by vapor diffusion of Pr^i_2O into a 1:1 solution of **4**·2PF$_6$ and **9** in MeCN. [**4**·**10**]·2PF$_6$: LSIMS: *m/z* 1167 $[M - PF_6]^+$, 1022 $[M - 2PF_6]^+$; HRLSIMS: *m/z* calc. for $[M - PF_6]^+$ ($C_{64}H_{66}F_6N_2O_{10}P$): 1167.4359, found: 1167.4315; ^{1}H NMR (CD_3CN): δ 3.75–3.81 (8H, m), 3.82–3.88 (8H, m), 3.93–4.08 (16H, m), 5.90–6.00 (6H, m), 6.15 (4H, t, *J* = 8.0 Hz), 6.23 (4H, m), 7.50–7.70 (6H, m), 7.88 (4H, d, *J* = 8.0 Hz), 8.15 (4H, s), 9.71 (4H, s); ^{13}C NMR (CD_3CN): δ 67.4, 68.6, 70.6, 71.9, 71.9, 105.3, 112.8, 117.8, 124.5, 125.0, 125.2, 129.8, 130.6, 130.7, 131.3, 142.0, 153.4. Crystals of [**4**·**10**]·2PF$_6$, suitable for X-ray structural analysis, were grown by vapor diffusion of Pr^i_2O into a 1:1 solution of **4**·2PF$_6$ and **10** in MeCN.

2,7-Bis(4-bromomethylbenzyl)diazapyrenium bis(hexafluorophosphate) (6·2PF$_6$)

A solution of **2** (0.5 g, 2.45 mmol) in MeCN (20 mL) was added dropwise to a solution of **5** (7.0 g, 26.6 mmol) in MeCN (200 mL) and the resulting mixture was heated under reflux for 12 h. After cooling to ambient temperature, the mixture was filtered and the solid residue was washed with Et_2O and dissolved in H_2O. Addition of NH_4PF_6 (5 g) caused the formation of a precipitate, which was filtered off to afford **6**·2PF$_6$ (1.92 g, 91%) as a bright yellow solid. mp = 248 °C (decomp.); LSIMS: *m/z* 717 $[M - PF_6]^+$; ^{1}H NMR (CD_3CN): δ 4.60 (4H, s), 6.25 (4H, s), 7.57 (4H, d, *J* = 9.5 Hz), 7.62 (4H, d, *J* = 9.5 Hz), 8.82 (4H, s), 9.95 (4H, s).

1,4-Bis(2,7-diazapyreniummethylene)benzene bis(hexafluorophosphate) (7·2PF$_6$)

A solution of **2** (350 mg, 1.70 mmol) and **5** (225 mg, 0.85 mmol) in MeCN (50 mL) was heated under reflux for 4 h. After cooling to ambient temperature, the mixture was filtered and the solid residue was washed with Et_2O and dissolved in H_2O–Me_2CO (25 mL). Addition of NH_4PF_6 (5 g) and evaporation of Me_2CO caused the formation of a precipitate, which was filtered off to afford **7**·2PF$_6$ (802 mg, 59%) as a yellow solid. mp > 280 °C; LSIMS: *m/z* 657 $[M - PF_6]^+$; ^{1}H NMR (CD_3CN): δ 6.18 (4H, s), 7.67 (4H, s) 8.48 (4H, d, *J* = 9.1 Hz), 8.68 (4H, d, *J* = 9.1 Hz), 9.64 (4H, s), 9.84 (4H, s).

Cyclophane 14·4PF$_6$

Method A. A solution of **6**·2PF$_6$ (150 mg, 0.17 mmol), **11** (30 mg, 0.19 mmol), and **13** (233 mg, 0.87 mmol) in DMF (10 mL) was stirred for 14 d at room temperature. The addition of Et_2O (50 mL) caused the formation of an orange precipitate, which was filtered off and dissolved in H_2O (20 mL). The resulting solution was subjected to liquid/liquid extraction (CH_2Cl_2) for 5 d. Addition of NH_4PF_6 (1 g) caused the formation of a precipitate which was filtered off to give **14**·4PF$_6$ (59 mg, 30%) as a yellow powder. mp > 290 °C (decomp.); LSIMS: *m/z* 1003 $[M - PF_6]^+$, 858 $[M - 2PF_6]^+$; HRLSIMS: *m/z* calc. for $[M - PF_6]^+$ ($C_{40}H_{32}F_{18}N_4P_3$): 1003.1552, found: 1003.1525; ^{1}H NMR (CD_3CN): δ 5.68 (4H, s), 6.21 (4H, s), 7.57 (4H, d, *J* = 8.0 Hz), 7.79 (4H, d, *J* = 8.0 Hz), 7.86 (4H, d, *J* = 7.0 Hz), 8.64 (4H, s), 8.74 (4H, d, *J* = 7.0 Hz), 9.90 (4H, s); ^{13}C NMR (CD_3CN): δ 65.6, 67.8, 127.9, 130.9, 131.1, 131.4, 137.3, 137.6, 141.4, 145.8, 149.2. Crystals, suitable for X-ray analysis, were grown by vapor diffusion of Pr^i_2O into an MeCN solution of **14**·4PF$_6$.

Method B. A solution of **2** (34 mg, 0.17 mmol), **12**·2PF$_6$ (136 mg, 0.16 mmol), and **13** (140 mg, 0.52 mmol) in DMF (10 mL) was subjected to a pressure of 12 kbar for 2 d at 20 °C.

The mixture was treated as described in Method A to give **14**·$4PF_6$ (80 mg, 42%) as a yellow powder.

Cyclophane 16·$4PF_6$

A solution of **2** (34 mg, 0.11 mmol), **6**·$2PF_6$ (100 mg, 0.10 mmol), and **15** (233 mg, 0.69 mmol) in DMF (25 mL) was stirred for 14 d at room temperature. The addition of Et_2O (50 mL) caused the formation of an orange precipitate which was filtered off and dissolved in H_2O (20 mL). The resulting solution was subjected to liquid/liquid extraction (CH_2Cl_2) for 5 d. Addition of NH_4PF_6 (1 g), caused the formation of a precipitate, which was filtered off to give **16**·$4PF_6$ (63.0 mg, 51%) as a yellow solid. mp > 280 °C (decomp.); LSIMS: *m/z* 1051 $[M - PF_6]^+$, 906 $[M - 2PF_6]^+$; HRLSIMS: *m/z* calc. for $[M - 2PF_6]^+$ ($C_{44}H_{32}F_{12}N_4P_2$): 906.1897, found: 906.1911; ^1H NMR (CD_3CN): δ 6.15 (8H, s), 7.53 (8H, s), 8.56 (8H, s), 9.69 (8H, s); ^{13}C NMR (CD_3CN): δ 67.6, 128.6, 130.8, 130.9, 131.5, 137.4, 141.5.

[2]Catenane 17·$4PF_6$

Method A. A solution of **2** (27 mg, 0.13 mmol), **12**·$2PF_6$ (100 mg, 0.12 mmol), and **9** (164 mg, 0.31 mmol) in MeCN (10 mL) was stirred for 14 d at room temperature. The addition of Et_2O (50 mL) caused the formation of a red precipitate, which was filtered off and dissolved in H_2O–Me_2CO (1:1, 25 mL). Addition of NH_4PF_6 (1 g), followed by the evaporation of Me_2CO, caused the formation of a precipitate, which was filtered off and washed with CH_2Cl_2 (10 mL) and Et_2O (1 × 10 mL). The resulting solid was dissolved in MeCN and precipitated by adding Et_2O. After four reprecipitations, **17**·$4PF_6$ (107 mg, 52%) was isolated as a red solid. mp > 300 °C; LSIMS: *m/z* 1539 $[M - PF_6]^+$, 1394 $[M - 2PF_6]^+$, 1249 $[M - 3PF_6]^+$; HRLSIMS: *m/z* calc. for $[M - PF_6]^+$ ($C_{68}H_{72}F_{18}N_4O_{10}P_3$): 1539.4171, found: 1539.4174; ^1H NMR (CD_3CN, 300 K): δ 2.63 (4H, br s), 3.10–3.14 (4H, m), 3.20–3.24 (4H, m), 3.57–3.61 (4H, m), 3.80–3.88 (8H, m), 4.01–4.15 (12H, m), 5.42 (4H, br s), 5.61 (4H, s), 6.18 (4H, s), 7.57 (4H, d, J = 7.0 Hz), 7.71 (4H, d, J = 8.0 Hz), 8.00 (4H, d, J = 8.0 Hz), 8.40 (4H, s), 8.71 (4H, d, J = 7.0 Hz), 9.83 (4H, s); ^{13}C NMR (CD_3CN, 304 K): δ 65.7, 66.9, 67.7, 68.5, 70.3, 70.6, 71.0, 71.3, 72.0, 72.2, 112.0, 114.4, 126.1, 126.7, 128.6, 129.9, 130.8, 130.9, 131.6, 132.2, 137.5, 138.1, 141.4, 145.2, 147.1, 149.3, 151.8. Crystals, suitable for X-ray analysis, were grown by vapor diffusion of Pr^i_2O into an MeCN solution of **17**·$4PF_6$.

Method B. A solution of **11** (30 mg, 0.19 mmol), **6**·$2PF_6$ (150 mg, 0.17 mmol), and **14** (200 mg, 0.37 mmol) in MeCN (10 mL) was stirred for 14 d at room temperature. The mixture was treated as described in Method A to afford **17**·$4PF_6$ (109 mg, 37%) as a red solid.

[2]Catenane 18·$4PF_6$

A solution of **2** (27 mg, 0.13 mmol), **12**·$2PF_6$ (100 mg, 0.12 mmol), and **10** (195 mg, 0.31 mmol) in DMF (4 mL) was stirred for 14 d at room temperature. The addition of Et_2O (50 mL) caused the formation of a red precipitate, which was filtered off and dissolved in H_2O–Me_2CO (25 mL). Addition of NH_4PF_6 (1 g), followed by the evaporation of Me_2CO, caused the formation of a precipitate, which was filtered off and purified by column chromatography (SiO_2 : DMF–2M NH_4Cl, 1:1) to afford **18**·$4PF_6$ (122 mg, 56%) as a purple solid. mp > 300 °C; LSIMS: *m/z* 1639 $[M - PF_6]^+$, 1495 $[M - 2PF_6]^+$, 1349 $[M - 3PF_6]^+$; ^1H NMR (CD_3CN, 333 K): δ 1.79 (2H, d, J = 11.0 Hz), 3.50–3.58 (2H, m), 3.65–3.83 (6H, m), 3.85–3.90 (4H, m), 3.93–4.17 (14H, m), 4.20–4.37 (6H, m), 5.53 (2H, t, J = 8.0 Hz), 5.62 and 5.70 (4H, ABq, J_{AB} = 13.0 Hz), 5.75 (2H, d, J = 8.0 Hz), 6.09 (2H, d, J = 7.0 Hz), 6.04 and 6.38 (4H, ABq, J_{AB} = 13.0 Hz), 6.71 (2H, t, J = 8.0 Hz), 6.75 (2H, t, J = 8.0 Hz), 6.84 (2H, m), 6.98 (2H, m), 7.88 and 8.06 (4H, ABq, J_{AB} = 8.0 Hz), 7.95 and 8.20 (4H, ABq, J_{AB} = 8.0 Hz), 8.03 (2H, s), 8.05 (2H, s), 8.44 (2H, d, J = 6.5 Hz), 8.60 (2H, d, J = 6.5 Hz), 9.21 (2H, s), 9.87 (2H, s); ^{13}C NMR (CD_3CN, 304 K): δ 66.0, 67.9, 68.7, 69.0, 70.7, 70.8, 71.3, 72.1, 72.6, 72.8, 105.0, 106.0, 107.4, 114.7, 123.3, 125.5, 126.1, 126.7, 127.9, 129.3, 129.7, 131.0, 132.1, 132.2, 132.6, 137.5, 137.6, 139.9, 141.5, 144.0, 145.7, 151.1, 153.8.

[2]Catenane 19·$4PF_6$

Method A. A solution of **2** (39 mg, 0.19 mmol), **6**·$2PF_6$ (150 mg, 0.17 mmol), and **9** (195 mg, 0.36 mmol) in DMF (10 mL) was stirred for 14 d at room temperature. The addition of Et_2O (100 mL) caused the formation of a red precipitate, which was filtered off and dissolved in H_2O–Me_2CO (1:1, 40 mL). Addition of NH_4PF_6 (1 g), followed by the evaporation of Me_2CO, caused the formation of a precipitate which was filtered off and washed with CH_2Cl_2 (10 mL) and Et_2O (1 × 10 mL). The resulting solid was dissolved in MeCN and precipitated by adding Et_2O. After three reprecipitations, the solid was crystallized from MeCN–Pr^i_2O to afford **19**·$4PF_6$ (221 mg, 73%) as a red solid. mp > 300 °C; LSIMS: *m/z* 1587 $[M - PF_6]^+$, 1442 $[M - 2PF_6]^+$, 1397 $[M - 3PF_6]^+$; ^1H NMR (CD_3CN, 313 K): δ 1.85 (4H, br s), 2.90–2.93 (4H, m), 3.04–3.07 (4H, m), 3.54–3.57 (4H, m), 3.80–3.86 (8H, m), 4.00–4.11 (12H, m), 5.32 (4H, s), 6.10 (8H, s), 7.91 (8H, br s), 8.29 (8H, br s), 9.71 (8H, s); ^{13}C NMR (CD_3CN, 304 K): δ 66.7, 66.8, 67.7, 68.3, 68.4, 70.2, 70.6, 70.9, 71.1, 71.3, 71.5, 71.9, 72.2, 110.4, 114.2, 130.1, 130.7, 130.9, 131.4, 131.9, 138.0, 138.7, 140.9, 142.3, 147.9, 151.6. Crystals, suitable for X-ray analysis, were grown by vapor diffusion of Pr^i_2O into a $MeNO_2$ solution of **19**·$4PF_6$.

Method B. A solution of **5** (33 mg, 0.13 mmol), **6**·$2PF_6$ (101 mg, 0.13 mmol), and **9** (140 mg, 0.26 mmol) in DMF (10 mL) was subjected to a pressure of 12 kbar for 3 d at 20 °C. The mixture was treated as described in Method A to afford **19**·$4PF_6$ (118 mg, 54%) as a red solid.

[2]Catenane 20·$4PF_6$

A solution of **2** (22 mg, 0.11 mmol), **6**·$2PF_6$ (100 mg, 0.10 mmol), and **10** (100 mg, 0.16 mmol) in DMF (10 mL) was stirred for 14 d at room temperature. The addition of Et_2O (100 mL) caused the formation of a red precipitate which was filtered off and dissolved in H_2O–Me_2CO (1 : 1, 40 mL). Addition of NH_4PF_6 (1 g) followed by the evaporation of Me_2CO caused the formation of a precipitate which was filtered off and washed with CH_2Cl_2 (10 mL) and Et_2O (1 × 10 mL). Purification of the residue by column chromatography (SiO_2 : DMF–2M NH_4Cl, 1:1) afforded **20**·$4PF_6$ (91 mg, 48%) as a purple solid. mp > 300 °C; LSIMS: *m/z* 1832 $[M]^+$, 1687 $[M - PF_6]^+$, 1542 $[M - 2PF_6]^+$, 1397 $[M - 3PF_6]^+$; HRLSIMS: *m/z* calc. for $[M - PF_6]^+$ ($C_{80}H_{76}F_{18}N_4O_{10}P_3$): 1687.4468, found: 1687.4487; ^1H NMR (CD_3CN, 273 K): δ 1.09 (2H, d, J = 8.0 Hz), 3.20–4.15 (28H, m), 4.16–4.50 (4H, m), 5.17 (2H, t, J = 8.0 Hz), 5.26 (2H, d, J = 8.0 Hz), 5.90–5.96

(4H, m), 6.05 (6H, s), 6.29 (2H, m), 6.46 (2H, d, $J = 8.0$ Hz), 6.58 (2H, t, $J = 8.0$ Hz), 7.76 (2H, d, $J = 9.0$ Hz), 7.86 (2H, d, $J = 8.0$ Hz), 7.90–8.10 (10H, m), 9.02 (2H, s), 9.43 (2H, s), 9.64 (2H, s), 9.68 (2H, s); ^{13}C NMR (CD_3CN, 304 K): δ 67.9, 68.7, 69.0, 70.7, 70.7, 70.8, 71.3, 72.0, 72.5, 72.9, 105.5, 105.8, 105.9, 114.6, 114.7, 125.9, 126.2, 129.4, 131.9, 132.0, 132.6.

1,8-Bis{4-(2-{2-[2-(2-hydroxyethoxy)ethoxy]ethoxy}ethoxy)-phenoxy}-3,6-dioxaoctane 22

A mixture of **21** (0.45 g, 1.32 mmol), 2-[2-(2-chloroethoxy)-ethoxy]ethanol (0.65 g, 3.86 mmol), and K_2CO_3 (1 g, 5.26 mmol) in MeCN (100 mL) was heated for 4 d under reflux and an atmosphere of N_2. After cooling to room temperature, the mixture was filtered and the residue was dissolved in CH_2Cl_2 (100 mL), washed with H_2O (2 × 50 mL), and dried ($MgSO_4$). The solvent was removed under reduced pressure and the residue was purified by column chromatography (SiO_2 : $CHCl_3$–Me_2CO, 9 : 1) to afford **22** (561 mg, 71%) as a white solid. mp = 77–78 °C; LSIMS 598: m/z $[M]^+$; ^{1}H NMR ($CDCl_3$): δ 2.54 (2H, br s), 3.56–3.65 (4H, m), 3.67–3.74 (16H, m), 3.80–3.85 (8H, m), 4.04–4.10 (8H, m), 6.83 (8H, s); ^{13}C NMR ($CDCl_3$): δ 61.8, 68.0, 68.1, 69.9, 70.4, 70.8, 70.9, 72.5, 115.6, 115.7, 153.1, 153.2.

1,8-Bis{4-(2-{2-[2-(2-tosyloxyethoxy)ethoxy]ethoxy}ethoxy)-phenoxy}-3,6-dioxaoctane 23

A solution of *p*-toluenesulfonyl chloride (0.96 g, 5.02 mmol) in CH_2Cl_2 (100 mL) was added dropwise to a solution of **22** (1.0 g, 1.67 mmol), Et_3N (1.52 g, 15.05 mmol), and DMAP (20 mg) in CH_2Cl_2 (200 mL) mantained at 0 °C under an atmosphere of N_2. The mixture was maintained at 0 °C for a further 12 h and washed with dilute HCl (50 mL) and H_2O (2 × 100 mL), and dried ($MgSO_4$). The solvent was removed under reduced pressure and the residue was purified by column chromatography (SiO_2 : CH_2Cl_2–MeOH, 99 : 1) to afford **23** (0.76 g, 50%) as a white solid. LSIMS: m/z 906 $[M]^+$; ^{1}H NMR ($CDCl_3$): δ 2.40 (6H, s), 3.55–3.90 (24H, m), 4.02–4.10 (12H, m), 6.82 (8H, s), 7.32 (4H, d, $J = 9.0$ Hz), 7.8 (4H, d, $J = 9.0$ Hz); ^{13}C NMR ($CDCl_3$): δ 21.6, 68.0, 68.1, 68.7, 69.3, 69.9, 70.7, 70.8, 70.9, 115.6, 115.7, 127.9, 129.8, 133.1, 144.8, 153.1, 153.2.

1,8-Bis{4-(2-{2-[2-{2-(4-tritylphenoxy)ethoxy}ethoxy]ethoxy}-ethoxy)phenoxy}-3,6-dioxaoctane 25

A mixture of **23** (0.54, 0.60 mmol), **24** (0.42 g, 1.25 mmol), and K_2CO_3 (1 g, 5.26 mmol) in MeCN (50 mL) was heated under reflux for 4 d. After cooling to room temperature, the mixture was filtered and the residue was washed with CH_2Cl_2 (30 mL). The solvent was removed under reduced pressure and the residue was dissolved in CH_2Cl_2 (100 mL), washed with H_2O (2 × 50 mL), and dried ($MgSO_4$). The solvent was removed under reduced pressure and the residue was purified by column chromatography (SiO_2 : $CHCl_3$–Me_2CO, 9 : 1) to give **25** (561 mg, 71%) as a white solid. LSIMS: m/z = 1235 $[M]^+$; ^{1}H NMR ($CDCl_3$): δ 3.74 (12H, s), 3.80–3.87 (12H, m), 4.03–4.12 (12H, m), 6.79 (4H, d, $J = 8.5$ Hz), 6.82 (8H, s), 7.08 (4H, d, $J = 8.5$ Hz), 7.14–7.29 (30H, m); ^{13}C NMR ($CDCl_3$): δ 64.3, 67.3, 68.1, 69.8, 69.9, 70.9, 77.2, 113.4, 115.6, 125.9, 127.4, 131.1, 132.2, 139.2, 147.1, 153.1, 156.8.

[2]Rotaxane 27·4PF$_6$

A solution of **5** (21 mg, 0.08 mmol), **7**·4PF$_6$ (64 mg, 0.08 mmol), **25** (197 mg, 0.16 mmol), and $AgPF_6$ (40 mg, 0.16 mmol) in MeCN (10 mL) was stirred for 14 d at ambient temperature. The addition of Et_2O (50 mL) caused the formation of a red precipitate which was dissolved in MeCN (6 mL) and reprecipitated by adding Et_2O. After four reprecipitations, the solid was crystallized from MeCN–Pr^i_2O to give **27**·4PF$_6$ (83 mg, 43%) as an orange solid. mp > 190 °C (decomp.); LSIMS: m/z 2287 $[M - PF_6]^+$, 2142 $[M - 2PF_6]^+$; HRLSIMS: m/z calc. for $[M - PF_6]^+$ ($C_{124}H_{114}F_{18}N_4O_{12}P_3$): 2285.7359, found: 2285.7514; ^{1}H NMR (CD_3CN, 300 K): δ 1.98–2.02 (4H, br s), 2.88–2.92 (2H, m), 2.98–3.02 (2H, m), 3.50–4.17 (32H, m), 5.94 (2H, d, $J = 8.5$ Hz), 6.01 (8H, s), 6.06 (2H, d, $J = 8.5$ Hz), 6.09 (2H, d, $J = 8.5$ Hz), 6.70 (2H, d, $J = 8.5$ Hz), 6.76 (2H, d, $J = 8.5$ Hz), 6.98–7.02 (4H, m), 7.09 (2H, d, $J = 8.5$ Hz), 7.14–7.28 (26H, m), 7.86 (8H, s), 8.34 (4H, s), 8.35 (4H, s), 9.70 (4H, s), 9.74 (4H, s); ^{13}C NMR (CD_3CN, 300 K): δ 64.9, 65.1, 66.9, 67.8, 67.9, 68.1, 68.3, 68.5, 68.8, 70.2, 70.3, 70.5, 71.0, 71.1, 71.2, 71.3, 71.4, 71.9, 72.0, 110.8, 113.6, 114.3, 115.0, 115.7, 116.1, 117.6, 126.2, 126.8, 128.3, 130.1, 130.8, 131.1, 131.5, 131.8, 132.0, 132.7, 132.9, 137.9, 139.8, 140.0, 141.3, 141.4, 147.7, 147.8, 148.0, 152.4, 153.6, 156.9, 157.9.

[2]Rotaxane 28·4PF$_6$

A solution of **5** (18 mg, 0.07 mmol), **25** (172 mg, 0.14 mmol), **26**·4PF$_6$ (46 mg, 0.07 mmol), and $AgPF_6$ (35 mg, 0.14 mmol) in MeCN (10 mL) was stirred for 14 d at ambient temperature. The addition of Et_2O (100 mL) caused the formation of a red precipitate which was filtered off and purified by column chromatography (MeOH–2M NH_4Cl–$MeNO_2$, 7 : 2 : 1) to give **28**·4PF$_6$ (37 mg, 23%) as a red solid. mp > 190 °C (decomp); LSIMS: m/z 2191 $[M - PF_6]^+$, 2046 $[M - 2PF_6]^+$, 1900 $[M - 3PF_6]^+$; HRLSIMS: m/z calc. for $[M - PF_6]^+$ ($C_{116}H_{114}F_{18}N_4O_{12}P_3$): 2189.7359, found: 2189.7300; ^{1}H NMR [$(CD_3)_2CO$, 243 K]: δ 3.55–4.20 (40H, m), 5.93 (8H, s), 6.33 (2H, d, $J = 9.0$ Hz), 6.46 (2H, d, $J = 9.0$ Hz), 6.53 (2H, d, $J = 9.0$ Hz), 6.83 (2H, d, $J = 9.0$ Hz), 6.89 (2H, d, $J = 9.0$ Hz), 7.04 (2H, d, $J = 9.0$ Hz), 7.12–7.32 (30H, m), 7.99 (8H, s), 8.02 (4H, d, $J = 5.0$ Hz), 8.24 (4H, d, $J = 5.0$ Hz), 9.28 (4H, d, $J = 6.3$ Hz), 9.32 (4H, d, $J = 6.3$ Hz); ^{13}C NMR [$(CD_3)_2CO$, 243 K]: δ 64.5, 64.9, 66.6, 66.8, 67.3, 67.4, 67.6, 69.8, 69.9, 70.4, 70.6, 70.6, 70.8, 71.1, 71.3, 71.6, 113.2, 113.3, 113.4, 113.6, 114.6, 115.2, 118.2, 126.1, 126.3, 126.6, 128.2, 128.4, 131.1, 131.3, 132.4, 132.5, 137.5, 139.2, 139.6, 145.3, 145.4, 145.4, 147.1, 147.5, 150.3, 150.5, 152.0, 153.3, 156.3, 157.3.

[2]Rotaxane 30·4PF$_6$

A solution of **2** (17 mg, 0.08 mmol), **9** (150 mg, 0.28 mmol), and **29** (134 mg, 0.20 mmol) in DMF (6 mL) was subjected to a pressure of 12 kbar for 3 d at 20 °C. The mixture was poured onto H_2O (60 mL) and a saturated aqueous NH_4PF_6 solution was added and the resulting suspension was extracted with $MeNO_2$ (2 × 25 mL). The organic layer was washed with H_2O (2 × 10 mL) and dried ($MgSO_4$). The solvent was removed under reduced pressure and the residue was purified by column chromatography (SiO_2 : MeOH–$MeNO_2$–CH_2Cl_2, 6 : 1 : 1) to afford **30**·4PF$_6$ (77 mg, 40%) as a deep orange solid. mp 195–198 °C; LSIMS : m/z 2018 $[M - 2PF_6]^+$; HRLSIMS: m/z calc. for $[M - 2PF_6]^+$ ($C_{132}H_{150}N_2O_{16}$) : 2019.0985, found: 2019.0945; ^{1}H NMR (CD_3CN): δ 1.26 (36H, s), 2.26 (6H, s), 3.10–3.15 (8H, m), 3.57–3.62 (8H, m), 3.65–3.90 (24H, m), 3.98–4.03 (4H, m), 4.13–4.18 (4H, m), 5.20 (8H, s), 6.28 (4H, s), 6.72 (4H, d, $J = 8.5$ Hz), 7.02–7.14 (24H, m), 7.26 (8H, d, $J = 8.5$ Hz), 7.77 (8H, d, $J = 8.5$ Hz), 8.49 (4H, s), 9.81 (4H, s); ^{13}C NMR (CD_3CN): δ 20.9, 31.6, 34.9, 64.1, 67.1, 68.3, 68.8, 70.3, 70.5, 70.6, 71.4, 71.6, 114.1, 114.3, 116.4, 118.3, 118.5, 125.4, 129.2,

Table 4 Crystal data, data collection, and refinement parameters for the [2]pseudorotaxanes $[\mathbf{3}\cdot\mathbf{9}]\cdot 2PF_6$, $[\mathbf{3}\cdot\mathbf{10}]\cdot 2PF_6$, $[\mathbf{4}\cdot\mathbf{9}]\cdot 2PF_6$, and $[\mathbf{4}\cdot\mathbf{10}]\cdot 2PF_6$[a]

Data	$[\mathbf{3}\cdot\mathbf{9}]\cdot 2PF_6$	$[\mathbf{3}\cdot\mathbf{10}]\cdot 2PF_6$	$[\mathbf{4}\cdot\mathbf{9}]\cdot 2PF_6$	$[\mathbf{4}\cdot\mathbf{10}]\cdot 2PF_6$
Formula	$[C_{44}H_{54}N_2O_{10}][PF_6]_2\cdot$ 2MeCN	$[C_{52}H_{58}N_2O_{10}][PF_6]_2\cdot$ MeCN · EtOAc	$[C_{56}H_{62}N_2O_{10}][PF_6]_2$	$[C_{64}H_{66}N_2O_{10}][PF_6]_2$
Formula weight	1142.9	1290.1	1213.0	1313.1
Colour, habit	Orange–red blocks	Red blocks	Yellow plates	Red blocks
Crystal size/mm	0.31 × 0.19 × 0.12	0.66 × 0.33 × 0.23	0.30 × 0.27 × 0.07	0.25 × 0.17 × 0.17
Crystal system	Triclinic	Monoclinic	Monoclinic	Triclinic
Space group	$P\bar{1}$ (no. 2)	$P2_1/n$ (no. 14)	$P2_1/c$ (no. 14)	$P\bar{1}$ (no. 2)
T/K	293	293	293	293
Cell dimensions				
a/Å	11.222(2)	15.655(3)	15.474(5)	13.799(3)
b/Å	11.277(3)	23.613(2)	13.197(4)	14.407(4)
c/Å	12.033(3)	17.177(2)	14.431(3)	16.336(5)
α/°	106.20(2)	—	—	110.09(2)
β/°	99.94(2)	102.04(2)	109.50(2)	90.33(2)
γ/°	107.20(2)	—	—	91.12(2)
V/Å^3	1342.0(5)	6210(2)	2778(1)	3049(1)
Z	1[b]	4	2[b]	2[c]
D_c/g cm^{-3}	1.414	1.380	1.450	1.430
$F(000)$	594	2688	1260	1364
μ/mm^{-1}	1.63	1.49	1.60	1.50
θ range/°	4.0–60.0	1.5–55.0	1.5–60.0	2.9–60.0
No. of unique reflections				
measured	3979	7791	4124	9056
observed, $\lvert F_o\rvert > 4\sigma(\lvert F_o\rvert)$	2850	5226	1803	4034
No. of variables	374	740	344	847
R_1[d]	0.068[e]	0.082[f]	0.106[f]	0.114[e]
wR_2[g]	0.181	0.089[h]	0.102[h]	0.297
Weighting factors a, b[i]	0.099, 1.673	0.0005[j]	0.0005[j]	0.185, 2.264
Largest diff. peak, hole/e Å^{-3}	0.38, −0.32	0.52, −0.47	0.66, −0.65	0.42, −0.39

[a] Details in common: graphite monochromated Cu-Kα radiation, ω-scans, Siemens P4 diffractometer. [b] The molecule has crystallographic C_i symmetry. [c] There are two crystallographically independent C_i symmetric molecules in the asymmetric unit. [d] $R_1 = \Sigma\lvert\lvert F_o\rvert - \lvert F_c\rvert\rvert/\Sigma\lvert F_o\rvert$. [e] Refinement based on F^2. [f] Refinement based on F. [g] $wR_2 = [\Sigma w(F_o^2 - F_c^2)^2/\Sigma w(F_o^2)^2]^{1/2}$. [h] The value quoted is for R_w. [i] $w^{-1} = \sigma^2(F_o^2) + (aP)^2 + bP$. [j] The value given is for g in $w^{-1} = \sigma^2(F) + gF^2$.

129.7, 130.8, 131.3, 131.5, 132.7, 132.8, 136.3, 140.7, 145.5, 149.5, 151.6.

Association constants

Method A. A 1:1 CD_3CN solution of host and guest was diluted [concentration (c) = 5×10^{-3}–1×10^{-4} M] in twenty consecutive steps. At each step, the chemical shift changes ($\Delta\delta$) of appropriate protons were determined by ^{1}H NMR spectroscopy. Non-linear curve-fitting[7] of the plot of $\Delta\delta$ *vs.* c gave the association constant (K_a).

Method B. Twenty CD_3CN solutions of host and guest were prepared by varying the concentration of the host (c_H) while maintaining that of the guest constant. For each solution, the absorbance (A) of the charge-transfer band associated with the complex was determined by UV-VIS spectroscopy. Non-linear curve-fitting[7] of the plot of A against c_H gave K_a.

X-Ray crystallography

Tables 4 and 5 summarize the crystal data, data collection, and refinement parameters for the dicationic compound $\mathbf{4}\cdot 2PF_6$, the [2]pseudorotaxanes $[\mathbf{3}\cdot\mathbf{9}]\cdot 2PF_6$, $[\mathbf{3}\cdot\mathbf{10}]\cdot 2PF_6$, $[\mathbf{4}\cdot\mathbf{9}]\cdot 2PF_6$, and $[\mathbf{4}\cdot\mathbf{10}]\cdot 2PF_6$, the tetracationic cyclophane $\mathbf{14}\cdot 4PF_6$, and the [2]catenanes $\mathbf{17}\cdot 4PF_6$ and $\mathbf{19}\cdot 4PF_6$. The data were collected on Siemens P4 diffractometers (with a rotating anode source for $\mathbf{14}\cdot 4PF_6$, $\mathbf{17}\cdot 4PF_6$ and $\mathbf{19}\cdot 4PF_6$), and the structures were solved by direct methods and refined by full matrix least-squares, based on F^2 for $\mathbf{4}\cdot 2PF_6$, $[\mathbf{3}\cdot\mathbf{9}]\cdot 2PF_6$, $[\mathbf{4}\cdot\mathbf{10}]\cdot 2PF_6$, $\mathbf{14}\cdot 4PF_6$, and $\mathbf{19}\cdot 4PF_6$, based on F for $[\mathbf{3}\cdot\mathbf{10}]\cdot 2PF_6$, $[\mathbf{4}\cdot\mathbf{9}]\cdot 2PF_6$, and $\mathbf{17}\cdot 4PF_6$. Disorder was found in the macrocyclic polyether components of $\mathbf{17}\cdot 4PF_6$ and $\mathbf{19}\cdot 4PF_6$ and in each case two 50% occupancy orientations were identified. In $\mathbf{17}\cdot 4PF_6$, all of these partial occupancy atoms were refined isotropically. In $\mathbf{19}\cdot 4PF_6$, they were refined anisotropically. Disorder was found in some of the hexafluorophosphate anions of $\mathbf{4}\cdot 2PF_6$, $[\mathbf{3}\cdot\mathbf{9}]\cdot 2PF_6$, $[\mathbf{4}\cdot\mathbf{10}]\cdot 2PF_6$, $\mathbf{14}\cdot 4PF_6$, $\mathbf{17}\cdot 4PF_6$, and $\mathbf{19}\cdot 4PF_6$, In each case, this disorder was resolved into two partial occupancy orientations with only the major occupancy atoms being refined anisotropically. The included solvent molecules in $\mathbf{4}\cdot 2PF_6$, $[\mathbf{3}\cdot\mathbf{9}]\cdot 2PF_6$, $\mathbf{17}\cdot 4PF_6$, $\mathbf{19}\cdot 4PF_6$, were found to be distributed over multiple full and partial occupancy sites. In $\mathbf{4}\cdot 2PF_6$ and $[\mathbf{3}\cdot\mathbf{9}]\cdot 2PF_6$, only the major occupancy non-hydrogen atoms were refined anisotropically. In $\mathbf{17}\cdot 4PF_6$, they were all refined isotropically and in $\mathbf{19}\cdot 4PF_6$ only the full occupancy non-hydrogen atoms were refined anisotropically. In each structure the [C–H] hydrogen atoms were placed in calculated positions, assigned isotropic thermal parameters, and allowed to ride on their parent atoms. The polarity of $\mathbf{14}\cdot 4PF_6$ could not be unambiguously determined. The slightly higher final values of R in $\mathbf{17}\cdot 4PF_6$ and $\mathbf{19}\cdot 4PF_6$ are a consequence of the high solvation and disorder in both the solvent and PF_6^- anious. The accuracies of the derived parameters vary by a factor of *ca.* 1.6 between the 'best' and 'worst' (super)structures. Computations were carried out using the SHELXTL PC program system.[15]

Table 5 Crystal data, data collection, and refinement parameters for the dicationic compound $\mathbf{4}\cdot 2PF_6$, the tetracationic cyclophane $\mathbf{14}\cdot 4PF_6$, and the [2]catenanes $\mathbf{17}\cdot 4PF_6$ and $\mathbf{19}\cdot 4PF_6$[a]

Data	$\mathbf{4}\cdot 2PF_6$	$\mathbf{14}\cdot 4PF_6$	$\mathbf{17}\cdot 4PF_6$	$\mathbf{19}\cdot 4PF_6$
Formula	$[C_{28}H_{22}N_2][PF_6]_2\cdot$ 1.5MeCN	$[C_{40}H_{32}N_4][PF_6]_4$	$[C_{68}H_{72}N_4O_{10}][PF_6]_4\cdot$ 4.5MeCN	$[C_{72}H_{72}N_4O_{10}][PF_6]_4\cdot$ $6MeNO_2$
Formula weight	738.0	1148.6	1869.9	2099.5
Colour, habit	Yellow blocks	Yellow octahedra	Red blocks	Red blocks
Crystal size/mm	0.40 × 0.33 × 0.33	0.33 × 0.23 × 0.20	0.57 × 0.50 × 0.40	0.60 × 0.33 × 0.25
Crystal system	Rhombohedral	Orthorhomic	Monoclinic	Monoclinic
Space group	$R\bar{3}$ (no. 148)	$Pna2_1$ (no. 33)	$C2/c$ (no. 15)	$C2/c$ (no. 15)
T/K	293	193	291	193
Cell dimensions				
a/Å	27.842(6)	15.109(2)	30.29(3)	28.925(3)
b/Å	—	24.224(2)	13.885(7)	13.581(1)
c/Å	12.445(4)	12.518(1)	26.88(2)	24.872(1)
α/°	—	—	—	—
β/°	—	—	122.79(2)	107.10(1)
γ/°	—	—	—	—
V/Å^3	8355(4)	4581.3(8)	9506(11)	9339(1)
Z	9[b]	4	4[c]	4[c]
D_c/g cm^{-3}	1.320	1.665	1.307	1.493
F(000)	3375	2304	3852	4320
μ/mm^{-1}	1.85	2.78	1.64	1.84
θ range/°	4.0–62.5	3.7–60.0	1.5–55.0	3.2–60.0
No. unique reflections				
measured	2960	3557	5983	6857
observed, $\lvert F_o\rvert > 4\sigma(\lvert F_o\rvert)$	2463	2769	3825	4292
No. of variables	268	661	555	724
R_1[d]	0.075[e]	0.073[e]	0.140[f]	0.127[e]
wR_2[g]	0.215	0.184	0.151[h]	0.338
Weighting factors a, b[i]	0.143, 18.326	0.124, 7.217	0.0005[j]	0.249, 47.796
Largest diff. peak, hole/e Å^{-3}	0.48, −0.41	0.58, −0.43	0.97, −0.47	0.79, −0.77

[a] Details in common: graphite monochromated Cu-Kα radiation, ω-scans, Siemens P4 diffractometer. [b] The molecule has crystallographic C_i symmetry. [c] The molecule has crystallographic C_2 symmetry. [d] $R_1 = \Sigma\lvert\lvert F_o\rvert - \lvert F_c\rvert\rvert/\Sigma\lvert F_o\rvert$. [e] Refinement based on F^2. [f] Refinement based on F. [g] $wR_2 = [\Sigma w(F_o^2 - F_c^2)^2/\Sigma w(F_o^2)^2]^{1/2}$. [h] The value quoted is for R_w. [i] $w^{-1} = \sigma^2(F_o^2) + (aP)^2 + bP$. [j] The value given is for g in $w^{-1} = \sigma^2(F) + gF^2$.

CCDC reference number 440/100. See http://www.rsc.org/suppdata/nj/1999/587/ for crystallographic files in .cif format.

Notes and references

1 For accounts, books and reviews on mechanically interlocked molecules and supermolecules, see: G. Schill, *Catenanes, Rotaxanes and Knots*, Academic Press, New York, 1971; D. M. Walba, *Tetrahedron*, 1985, **41**, 3161; C. O. Dietrich-Buchecker and J.-P. Sauvage, *Chem. Rev.*, 1987, **87**, 795; Y. S. Lipatov, T. E. Lipatova and L. F. Kosyanchuk, *Adv. Polym. Sci.*, 1989, **88**, 49; J.-P. Sauvage, *Acc. Chem. Res.*, 1990, **23**, 319; C. O. Dietrich-Buchecker and J.-P. Sauvage, *Bioorg. Chem. Front.*, 1991, **2**, 195; H. W. Gibson and H. Marand, *Adv. Mater.*, 1993, **5**, 11; J.-C. Chambron, C. O. Dietrich-Buchecker and J.-P. Sauvage, *Top. Curr. Chem.*, 1993, **165**, 131; F. Bickelhaupt, *J. Organomet. Chem.*, 1994, **475** 1; H. W. Gibson, M. C. Bheda and P. T. Engen., *Prog. Polym. Sci.*, 1994, **19**, 843; D. B. Amabilino, I. W. Parsons and J. F. Stoddart, *Trends Polym. Sci.*, 1994, **2**, 146; D.B. Amabilino and J. F. Stoddart, *Chem. Rev.*, 1995, **95**, 2725; Vögtle, T.Dünnwald and T. Schmidt, *Acc. Chem. Res.*, 1996, **29**, 451; A. C. Benniston, *Chem. Soc. Rev.*, 1996, **25**, 427; M. Fujita and K. Ogura, *Coord. Chem. Rev.*, 1996, **148**, 249; M. Belohradsky, F. M. Raymo and J. F. Stoddart, *Collect. Czech. Chem. Commun.*, 1996, **61**, 1; F. M. Raymo and J. F. Stoddart, *Trends Polym. Sci.*, 1996, **4**, 208; R. Jäger and F. Vögtle, *Angew. Chem., Int. Ed. Engl.*, 1997, **36**, 930; M. Belohradsky, F. M. Raymo and J. F. Stoddart, *Collect. Czech. Chem. Commun.*, 1997, **62**, 527; S. A. Nepogodiev and J. F. Stoddart, *Chem. Rev.*, 1998, **98**, 1959; J.-C. Chambron and J.-P. Sauvage, *Chem. Eur. J.*, 1998, **4**, 1362.

2 For accounts and reviews on template-directed syntheses of catenanes and rotaxanes relying on a combination of [C–H···O] hydrogen bonds, [π···π] stacking, and [C–H···π] interactions, see: D. Philp and J. F. Stoddart, *Synlett*, 1991, 445; D. Pasini, F. M. Raymo and J. F. Stoddart, *Gazz. Chem. Ital.*, 1995, **125**, 431; F. M. Raymo and J. F. Stoddart, *Pure Appl. Chem.*, 1996, **68**, 313; D. B. Amabilino, F. M. Raymo and J. F. Stoddart, *Comprehensive Supramolecular Chemistry*, ed. M. W. Hosseini and J.-P. Sauvage, Pergamon, Oxford, 1996, vol. 9, p. 85; R. E. Gillard, F. M. Raymo and J. F. Stoddart, *Chem. Eur. J.*, 1997, **3**, 1933; F. M. Raymo and J. F. Stoddart, *Pure Appl. Chem.*, 1997, **69**, 1987; F. M. Raymo and J. F. Stoddart, *Chemtracts*, 1998, **11**, 491.

3 R. Ballardini, V. Balzani, A. Credi, M. T. Gandolfi, S. J. Langford, S. Menzer, L. Prodi, J. F. Stoddart, M. Venturi and D. J. Williams, *Angew. Chem., Int. Ed. Engl.*, 1996, **35**, 978; P. R. Ashton, S. J. Langford, N. Spencer, J. F. Stoddart, A. J. P. White and D. J. Williams, *Chem. Commun.*, 1996, 1387; A. C. Benniston, A. Harriman and D. S. Yufit, *Angew. Chem., Int. Ed. Engl.*, 1997, **36**, 2356; A. Credi, V. Balzani, S. J. Langford and J. F. Stoddart, *J. Am. Chem. Soc.*, 1997, **119**, 2679; A. Credi, V. Balzani, S. J. Langford, M. Montalti, F. M. Raymo and J. F. Stoddart, *New J. Chem.*, 1998, 1061.

4 S. Hünig, J. Grosse, E. F. Lier and H. Quast, *Liebigs Ann. Chem.*, 1973, 339.

5 B. L. Allwood, N. Spencer, H. Shahriari-Zavareh, J. F. Stoddart and D. J. Williams, *J. Chem. Soc., Chem. Commun.*, 1987, 1064.

6 P. R. Ashton, E. J. T. Chrystal, J. P. Mathias, K. P. Parry, A. M. Z. Slawin, N. Spencer, J. F. Stoddart and D. J. Williams, *Tetrahedron Lett.*, 1987, **28**, 6367.

7 K. A. Connors, *Binding Constants*, Wiley, New York, 1987.

8 For a definition of the term 'co-conformation', see: M. C. T. Fyfe, P. T. Glink, S. Menzer, J. F. Stoddart, A. J. P. White and D. J. Williams, *Angew. Chem., Int. Ed. Engl.*, 1997, **36**, 2068.

9 J. Sandström, *Dynamic NMR Spectroscopy*, Academic Press, London, 1982.

10 I. O. Sutherland, *Annu. Rep. NMR Spectrosc.*, 1982, **4**, 71.

11 P. R. Ashton, R. Ballardini, V. Balzani, M. Belohradsky, M. T. Gandolfi, D. Philp, L. Prodi, F. M. Raymo, M. V. Reddington, N. Spencer, J. F. Stoddart, M. Venturi and D. J. Williams, *J. Am. Chem. Soc.*, 1996, **118**, 4931.

12 D. D. Perrin and W. L. Armarego, *Purification of Laboratory Chemicals*, Pergamon Press, New York, 3rd edn., 1988.

13 P.-L. Anelli, P. R. Ashton, R. Ballardini, V. Balzani, M. Delgado, M. T. Gandolfi, T. T. Goodnow, A. E. Kaifer, D. Philp, M. Pietraszkewicz, L. Prodi, M. V. Reddington, A. M. Z. Slawin, N.

Spencer, J. F. Stoddart, C. Vicent and D. J. Williams, *J. Am. Chem. Soc.*, 1992, **114**, 193.
14 M. Asakawa, P. R. Ashton, S. E. Boyd, C. L. Brown, R. E. Gillard, O. Kocian, F. M. Raymo, J. F. Stoddart, M. S. Tolley, A. J. P. White and D. J. Williams, *J. Org. Chem.*, 1997, **62**, 26.
15 SHELXTL PC version 5.03, Siemens Analytical X-Ray Instruments, Inc., Madison, WI, 1994.

Paper 8/09433K